11-29-2023 1:30 PM

Characterizing the Spatial Distribution of Inhibitory Interneurons Across Early Sensory and Association Areas in Callithrix jacchus

Nika Khajehdehi,

Supervisor: Martinez-Trujillo, Julio, *The University of Western Ontario*
A thesis submitted in partial fulfillment of the requirements for the Master of Science degree in Physiology and Pharmacology
© Nika Khajehdehi 2023

Abstract

The prefrontal cortex (PFC) is one of the cortical areas responsible for complex cognitive abilities, a function that is believed to arise from increased persistent activity within its microcircuits. Activity within microcircuits is regulated by parvalbumin-containing (PV), calbindin-containing (CB), and calretinin-containing (CR) inhibitory interneurons (INs). It remains unclear how the distribution of activity-regulating INs differs across cortical areas such that persistent activity increases specifically within association areas, allowing for their complex functions. This thesis aims to address this gap by characterizing the spatial distributions and differences in relative proportions of INs across early sensory areas and association areas of the common marmoset (*Callithrix jacchus)*. Immunohistochemical analysis of INs across sensory and association areas was performed, followed by manual cell counting. I observed less activity-suppressing PV interneurons and more activity-inducing CR interneurons from sensory areas to PFC. These findings suggest a hierarchical gradient in INs across cortical areas exist and may contribute to the mechanism underlying PFC's functions.

Keywords

Summary for Lay Audience

The prefrontal cortex (PFC) is an association area of the outer division of the brain, the cortex, involved in regulating thoughts, decisions, and actions through connections with other brain areas. A region within the PFC, known as the dorsolateral PFC (LPFC), is involved in temporary storage of information while the brain uses that information. This is an ability known as working memory (WM) and can guide our decisions and behaviours. While many species have WM ability, primates demonstrate advanced WM capabilities. WM ability is thought to be associated with increased levels of activity within LPFC compared with other brain areas. At the cellular level, increased activity in LPFC compared with sensory areas is thought to arise, at least in part, from differences in the abundances of specific cells responsible for regulating activity levels across the cortex, known as interneurons (INs), but the exact nature of such changes in cellular abundance across brain areas remains unclear. Given that different types of INs have different effects on overall activity levels, this project aimed to compare distributions and proportions of different INs between other sensory and association areas to understand the cellular mechanism underlying increased LPFC activity levels during WM in primates, specifically in marmosets in the context of this project. The findings revealed an increase in activity-promoting IN and a decrease in activity-inhibiting IN relative proportion from early areas to LPFC, providing support for the theory that changes in IN proportions may be involved in the emergence of increased LPFC activity during WM.

Acknowledgements

I would like to express my gratitude and acknowledge the efforts of all those who have contributed to the completion of this research project in numerous ways.

First and foremost, I would like to thank my supervisor, Dr. Julio Martinez-Trujillo, for his patience, support, guidance, and insight throughout the course of the project and for resources and equipment that has been dedicated to the generation and completion of this project.

I would like to thank the JMT and Inoue labs for providing a stimulating and collaborative environment to conduct research in. These qualities have helped me countless times to overcome obstacles and push through the challenges that often arise throughout the course of a research project. I would specifically like to thank Michelle Jimenez-Sosa for showing me the ropes during my time as a newcomer to the lab and for giving me opportunities to learn about various laboratory techniques. I would also like to specifically thank Michael Feyerabend for his invaluable guidance and contributions to the methodology optimization and statistical analysis components of this Masters project.

I would like to thank my advisory committee members Dr. Jane Rylett, Dr. Arthur Brown and Dr. Wataru Inoue for the guidance and feedback they have provided to help me continuously improve the quality of my work.

Finally, I would like to thank my friends and family for their patience, support, and encouragement throughout my Masters. You have motivated me to continue pushing forward, even throughout the most challenging of times.

Abbreviations

WM = working memory

V1 = primary visual cortex

LIP = lateral intraparietal cortex

PFC = prefrontal cortex

DLPFC = dorsolateral prefrontal cortex

gPFC = granular PFC

GABA = γ-aminobutyric acid

WM = working memory

PC = pyramidal cells

PV = parvalbumin

CR = calretinin

CB = calbindin

SST = somatostatin

VIP = vasoactive intestinal peptide

LPFC = lateral prefrontal cortex

MT = middle temporal area

MST = medial superior temporal area

PFA = paraformaldehyde

O.C.T. = optimal cutting temperature

PBS = phosphate-buffered saline

ROI = region of interest

NG = neurogranin

CGE = central ganglionic eminence

LGN = lateral geniculate nucleus

STM = short-term memory

Table of Contents

List of Tables

List of Figures

1 – Introduction

1.1 *Types of neurons in the cortex*

Neurons are considered to be the structural and functional units of the brain as they communicate with one another to process information (Baslow, 2011). There are an extensive number of ways to categorize neurons as they can be distinguished by their anatomical, morphological, and/or physiological properties. One of the simplest methods of distinction between subtypes of neurons is based on their excitatory vs. inhibitory capabilities.

1.2 *Excitatory and inhibitory neurons*

Within the context of the cerebral cortex, the effect of a neuron's output on its target is dependent on the neurotransmitter that it releases. Although the type of neurotransmitter alone does not dictate whether a neuron is excitatory or inhibitory, in the mammalian neocortex one could consider the majority of the neurons releasing glutamate are excitatory and those releasing γ-aminobutyric acid (GABA) are inhibitory. Pyramidal cells (PCs) are one type of excitatory neuron of the cortex and release the neurotransmitter glutamate. Inhibitory neurons of the cortex, on the other hand, are referred to as interneurons and primarily release GABA. Across these two categories of cortical neurons, excitatory PCs are the more abundant of the two and account for approximately 70-90% of the primate cortical neuron population, while inhibitory interneurons account for the remaining 10-30% of the neuron population (Bianchi et al., 2013; Kooijmans et al., 2020).

1.3 Working memory and attention

Working memory (WM) refers to the ability to mentally represent and manipulate information during a period of sustained attention even in the absence of sensory stimulus. While short-term memory (STM) is a component of WM, the two are not the same. STM allows for the temporary retention of information in sensory cortices on the scale of seconds in the absence of attention. WM, on the other hand, is dependent on sustained attention and therefore its contents are susceptible to interference by distractions. Due to the attention-dependent nature of WM, its duration can vary greatly between individuals and species (Cela-Conde et al., 2014).

While several species demonstrate STM and components of WM to a certain extent, primates, humans in particular, demonstrate a highly advanced level of this ability due to increased capacity for information retention and increased ability to sustain attention (Qi, 2010; Cela-Conde et al., 2014; Constantinidis et al., 2018;).

One major underlying structure that is thought to be involved in WM ability is the dorsolateral prefrontal cortex, a region of the granular PFC (gPFC) that was found to have undergone evolutionary expansion in primates (D'esposito et al., 1995; Kimberg et al., 1997; Manoach et al., 1997; Mars & Grol, 2007; Torres-Gomez et al., 2020). Reports of bilateral lesions in the prefrontal cortex of rhesus macaques causing impairments in delayed-response task performance supports the role of prefrontal cortex in working memory ability. However, the sole possession of a dorsolateral prefrontal cortex is not sufficient to give rise to such a complex cognitive ability. Goldman-Rakic et al. (1995) reported sustained activity of PFC neurons during the delay period of delayed-response tasks in monkeys. More recent studies have provided further support for the association

between working memory and continuous activity of local networks of neurons, also known as microcircuits, within the association areas of the brain, such as the prefrontal and parietal cortices (Finn et al., 2019) and a visual delayed-response task in macaque monkeys uncovered activity persisting into the delay period in LPFC neurons but not in MT neurons (Mendoza-Halliday et al., 2014)

The prefrontal cortex plays a vital role in carrying out complex cognitive processes, such as planning and problem-solving (Koechlin et al., 1999), while the parietal cortex plays a role in modulating selective attention, spatial perception, and eye movement in response to visual stimuli (Bushnell et al., 1981; Uncapher et al., 2009; Malhotra et al., 2009). Microcircuits play a vital role in regulating excitatory and inhibitory signals within not only the above-mentioned association areas, but all over the brain.

1.4 Cortical microcircuit organization

Microcircuits contain four main cell types: excitatory pyramidal cells (PC) and three subtypes of inhibitory interneurons. Recurrent activity within microcircuits arises from continuous excitation of PC, while each of the interneuron subtypes play a role in regulating PC activity (Wang et al., 2004; Wang & Yang, 2018). The three interneuron subtypes are distinguished by their non-overlapping calcium-binding protein content; calbindin-containing (CB), calretinin-containing (CR), and parvalbumin-containing (PV) interneurons (Condé et al., 1994; Wang et al., 2004). Their non-overlapping nature allows for each IN's spatial distribution to be characterized immunohistochemically by using calcium-binding protein markers and performing colocalization analysis to ensure distinct subpopulations of INs are being observed.

PV target the soma of PCs and inhibit their activity, CB target PC dendrites to inhibit inputs to the cell, and CR inhibit CB, removing inhibitory input to PCs. Overall, CB and PV have a net inhibitory effect while CR has a net excitatory effect, also known as a disinhibitory effect, on PC (Wang & Yang, 2018, Fig. 1A). The functional relevance of these connectivity patterns has been characterized by Wang et al. (2004); PV cells provide generalized inhibition across relatively large areas due to their target being at the level of the soma, while CR cells provide disinhibition to localized, relatively smaller regions of the cortex due to their target being the dendrite-targeting CB cells. The role of CB cells is to prevent distracting stimuli from disrupting the neuronal network displaying persistent activity. Overall, the interplay between different interneurons contributes to modulation of cortical activity levels therefore plays a vital role in the regulating levels of persistent activity across the cortex.

In rodents, the inhibitory interneurons are characterized by a different set of proteins; somatostatin-containing interneurons (SST), vasoactive intestinal peptide-containing interneurons (VIP), and the previously mentioned PV-containing interneurons. The SST interneurons in rodents are thought to be equivalent to CB interneurons in primates, while VIP interneurons in rodents are thought to be equivalent to CR interneurons in primates (Kubota et al., 1994; Kawaguchi and Kubota, 1997; Petilla Interneuron Nomenclature Group et al., 2008).

Scientists over the past several decades have uncovered the functions of specific brain regions in primates and characterized the cells contained within cortical microcircuits, but one critical question remains unanswered: how do microcircuits in early sensory areas, such as the primary visual cortex, differ from those in association areas such that more persistent activity is able to occur in association areas during complex cognitive functions?

There is a gap in current scientific knowledge regarding how microcircuits in the dorsolateral PFC compare to those in other brain regions.

1.5 Laminar distributions of cortical interneurons

The cerebral cortex is arranged into six layers, cortical layer I being the most superficial layer closest to the pia and layer VI being the innermost layer closest to the white matter. Cortical layer I primarily contains axons, dendrites, and axon terminals of neurons with their somata located in deeper layers. Cortical layers II and III are supragranular layers and mostly contain small PCs. PCs within these layers are involved in both intra- and inter-areal communication as their axons project to local neurons and neurons of other cortical areas. Cortical layer IV is known as the internal granular layer and is most prominent in sensory areas as it is the major site of sensory input from the thalamus. Cortical layer V contains PCs that mainly give rise to major output pathways of the cortex and therefore project to other cortical areas and subcortical structures. Layer VI contains heterogenous neurons and carries axons of neurons to other cortical areas (Miyashita, 2022).

The interneurons of the cortex have characteristic laminar distributions as each subtype primarily localizes to specific cortical layers. Past studies have found that PV primarily localizes to cortical layer IV (Van Brederode et al., 1990; DeFelipe et al., 1999; Goodchild and Martin, 1998; Hof et al., 1998; Bourne et al., 2007) while CR and CB primarily localize to supragranular layers II and III (Condé et al., 1994; Goodchild and Martin, 1998; Hof et al., 1998, Bourne et al., 2007; Fig. 1A).

1.6 Aims and rationale of the current study

The current study aims to explore these matters by assessing the relative cell type proportions of PV, CR, and CB interneurons across one of many information processing pathways in *Callithrix jacchus,* hereafter referred to as common marmosets (Fig. 1B). A gradient in the cell type abundance across cortical regions may be a reflection of a difference in excitation-inhibition balance across the brain, which may ultimately account for the complexity gradient across brain regions.

The specific pathway that the current study will focus on is a component of the dorsal visual information processing stream that includes the primary visual cortex (V1), lateral inferior parietal cortex (LIP/7a) and lateral prefrontal cortex (LPFC/8aD). This stream is responsible for spatial- and action-related processing such as motion detection and eye movements (van Polanen and Davare, 2015). The primary visual cortex is an early sensory area responsible for receiving information about visual stimuli via projections from the lateral geniculate nucleus (LGN) of the thalamus, while LIP and LPFC regions are
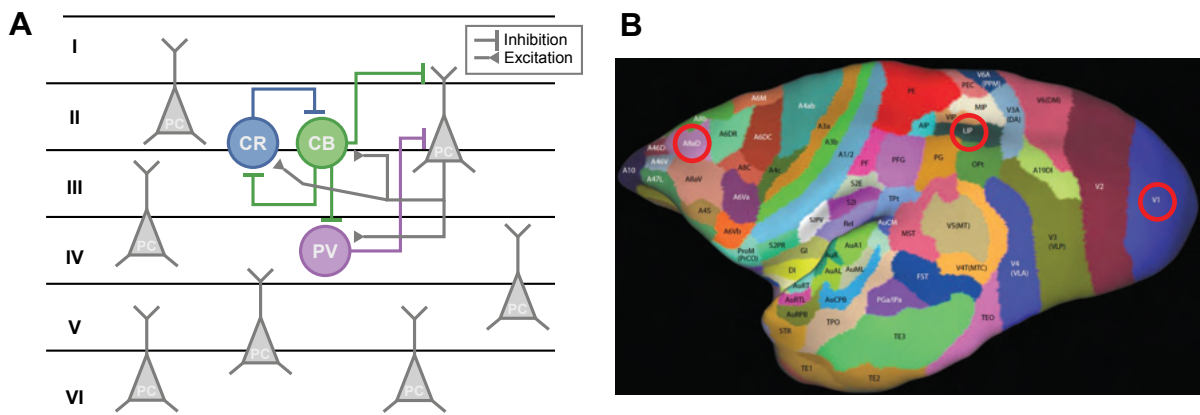
Figure 1. Simplified representation of microcircuit organization and connectivity among INs and PCs in the neocortex. INs shown in their respective cortical layers of highest abundance for illustration purposes (**A**). Locations of V1, LIP, and lateral PFC/area 8aD on a marmoset brain (**B**).

higher order association areas responsible for processing and mentally representing information. LIP plays a role in spatial attention and planning eye movements (Bisley and Goldberg, 2003; Bisley et al., 2011).

Marmosets are becoming increasingly popular animal models in the field of neurophysiology, particularly in applications involving behaviour, visual information processing, and working memory (Feizpour et al., 2021). The marmoset brain offers experimental advantages due to its small size and smooth arrangement which are particularly advantageous in the study of cell type diversity, dissection, and study of neural circuitry (Miller et al., 2016). In addition, the core aspects of visual processing were found to be conserved across monkeys and humans (Kell et al., 2023) which, in conjunction with their experimental advantages, makes marmosets an ideal animal model for the study of visual neuroscience.

Due to marmosets' increasing popularity in the field of cognition and its experimental advantages that allow for a wide variety of experimental approaches within a single animal model, it is fundamental that we develop a thorough understanding of the structure and organization of the marmoset cortex as these contribute to the foundational basis that future studies can expand upon. By characterizing the interneuron composition and microcircuit organization across cortical areas in these species the findings of the current study contribute to our foundational understanding of interneuron distribution and abundance across sensory and association areas in this animal model.

1.7 Direct comparison to past findings

A past study by Torres-Gomez et al. (2020) has characterized the proportions of PV, CB, and CR interneurons across middle temporal (MT), medial superior temporal

(MST), and the lateral prefrontal cortex (LPFC) in cortical layers II/III of rhesus macaques. MT is an early visual area of the dorsal stream involved in motion processing and receives inputs from multiple cortical areas, including LGN and visual cortices V1 and V2 (Goodale 1993; Lui and Rosa, 2015; Sheth and Young, 2016). MST is downstream to MT and integrates visual motor signals from MT and receives projections from other cortical areas involvement in eye movement, such as the superior colliculus, LIP, and frontal eye fields (Goodale, 1993; Verghese and Beutter, 2002).

Torres-Gomez et al., found that the proportion of PV in cortical layers II/III decreased, while the proportion of CR cells increased from MT/MST to LPFC. Although the cortical areas and animal models in the current study are different than those studied by Torres-Gomez et al., we still expect to observe a similar, if not more pronounced, gradient in PV and CR proportions from V1 to PFC considering V1 is an earlier sensory area that is more cytoarchitecturally distant from LPFC relative to MT/MST (Fig. 2).

In addition, the current study aims to expand upon the existing findings by Torres-Gomez et al. by assessing inhibitory interneuron proportions across all cortical layers rather than only layers II/III. This development has major implications in the interpretation of results because it accounts for the characteristic laminar distributions of each interneuron subtype; CR and CB are abundant in superficial cortical layers, layers II/III, while PV is most abundant in deeper cortical layers below layers II/III (Van Brederode et al., 1990; Goodchild and Martin, 1998; Hof et al., 1998; DeFelipe et al., 1999; Bourne et al., 2007).

Furthermore, the current study explores interneuron proportions across a pathway that spans a more diverse range of cortical areas including a sensory area, a parietal association area, and a frontal association area. In contrast, the study by Torres-Gomez et

al. spans only two temporal association areas and one frontal association area. Including a more diverse range of cortical areas in the current study allows us to assess interneuron proportion gradients more effectively since there is a greater contrast in the hierarchy of
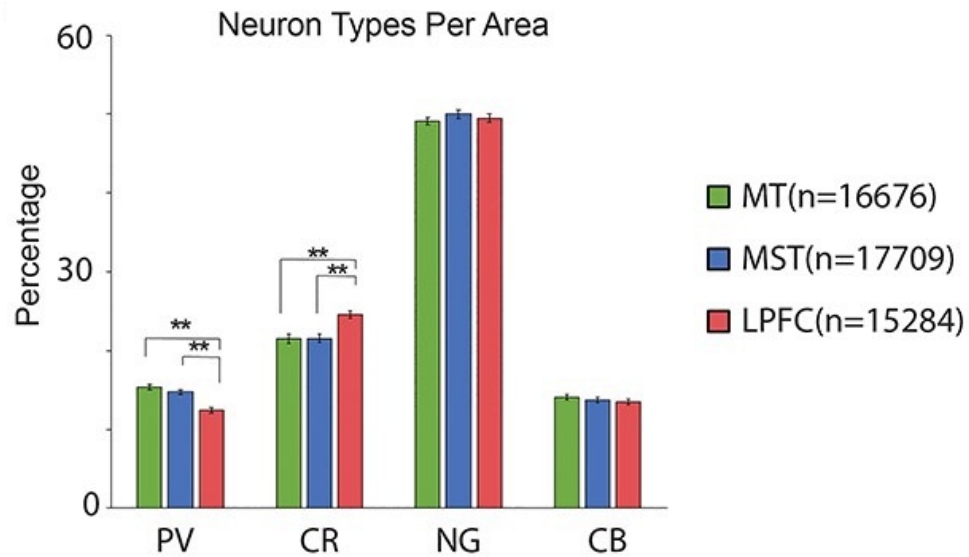
Figure 2. Findings of study by Torres-Gomez et al. (2020). Percentages of PV, CB, CR, and neurogranin (NG) in layer II/III across MT, MST, and LPFC are shown. Significant differences are shown by brackets marked with asterisks.

area complexity across the areas included in the current study.

Additionally, the current study places a greater emphasis on optimizing the cell counting method to ensure an accurate cell count that is representative of the true interneuron abundance is achieved. The study by Torres-Gomez et al. did not account for antibody penetration levels and imaging limitations prior to manual cell counting, increasing the likelihood for interneuron proportions to misrepresented.

1.8 Importance of understanding microcircuit organization

The purpose of these microcircuits extends beyond that of solely driving working memory tasks. Disruptions in interneuron activity have been found to result in an imbalance in excitation and inhibition, ultimately giving rise to neurological disorders such as schizophrenia and epilepsy (Beasley & Reynolds, 1997; Torres-Gomez et al., 2020). In order to understand the full extent of the underlying pathophysiology associated with such disorders, we must first develop a thorough understanding of the physiological properties of cortical microcircuits and their molecular components in non-pathological states.

1.9 Overall objective and hypothesis

In order to understand the molecular processes that are responsible for regulating excitatory and inhibitory signals in the cortex, basic characteristics of molecular components involved in such processes must first be determined. The current study aims to uncover the spatial distribution of microcircuit cell types that give rise to persistent activity in association areas (Fig. 1A, B). The objective is to characterize the relative proportion of calbindin-containing, calretinin-containing, and parvalbumin-containing interneurons across V1, LIP/7a, and LPFC in marmosets. We expect that there will be an increase in the relative proportion of CR and a decrease in the relative proportions of PV and CB in accordance with increasing complexity across V1, LIP/7a, and LPFC cortical regions of marmosets.

2 – Methods

2.1 Ethics Statement

The animal care and handling procedures, encompassing basic care, housing and husbandry, animal training, surgical procedures, and experiments (data collection), were granted approval by the University of Western Ontario Animal Care Committee. This approval guarantees adherence to federal (Canadian Council on Animal Care), provincial (Ontario Animals in Research Act), regulatory (e.g., CIHR/NSERC), and other national CALAM standards, ensuring the ethical use of animals. The animals' physical and psychological well-being was regularly assessed by researchers, registered veterinary technicians, and veterinarians.

2.2 Animal subjects and tissue preparation

Two adult male marmosets were anesthetized and intracardially perfused with 4% paraformaldehyde (PFA). The brains were removed and stored in 4% PFA until they underwent preparation for immunohistochemistry.

The hemispheres of each brain were separated by a midsagittal cut. The three cortical areas of interest; V1, LIP/area 7a, and DLPFC/area A8aD; were identified in both hemispheres of each brain using figures the marmoset brain atlas (Paxinos et al., 2012) as a reference; figures 9b, 141b, and 189b were used as references for V1, LIP/area 7a, and DLPFC/area A8aD, respectively. V1 was readily identifiable by its characteristic densely-stained cortical layer IV. LIP was identified by its relative location to the intraparietal sulcus. DLPFC/Area A8aD was identified as the region lateral to the dorsal peak of the tissue opposite the orbital sulcus.

The hemispheres were cut into three individual blocks, each block containing one of the cortical areas of interest. Each block was submerged in sucrose cryoprotectant solution. The blocks were then placed into a cryomold and submerged in optimal cutting temperature (O.C.T.) compound. The cryomold units were lowered into isopentane cooled to approximately -50ºC to flash freeze the tissue embedded in O.C.T. compound. The embedded tissue blocks were each sliced into 40 µm-thick coronal sections using a Leica CM350 cryostat.

2.3 Immunohistochemistry

To quantify the abundance of each interneuron subtype within each slice based on their calcium-binding protein content, immunohistochemical procedures similar to those presented by Pollock et al. (2014) were followed. Tissue sections were first washed with three rounds of phosphate-buffered saline (PBS) washes, five minutes each, to remove any excess O.C.T. and cryoprotectant solution. Tissue sections were then permeabilized with two rounds of PBS with 2% Triton X-100 incubation for five minutes each. Next, tissue sections underwent a one-hour incubation with blocking solution containing 0.25% bovine serum albumin and 10% normal donkey serum diluted in PBS with 0.1% Triton X-100. Next, the primary antibodies were applied. Antibody combinations were limited to a maximum of three per stained section to allow for sufficient spectral separation among the dyes during the imaging process. As a result, immunohistochemistry was performed using one of two primary antibody combinations (Table 1, Fig. 3). The tissues were incubated overnight at 4 ºC in their respective antibody combinations.

The next day, three five-minute washes with PBS with 0.1% Triton X-100 were carried out. Next, the secondary antibodies conjugated to fluorophores were diluted to a

working concentration of 1:500 and applied to all tissue sections, then left to incubate in the dark for two hours. The secondary antibodies used were AlexaFluor 488 donkey anti-mouse, AlexaFluor 546 donkey anti-sheep, and AlexaFluor 647 donkey anti-rabbit. Next, the tissue sections were washed three times for five minutes each with PBS and 0.1% Triton X-100 followed by a 10-minute incubation in the dark with 1:5000 DAPI to stain nuclei within tissue sections. Tissue sections then underwent three final five-minute washes with PBS and were mounted on glass slides using Aqua-Poly/Mount mounting medium.

Condition	Antibody	Source
CONDITION 1	1:1000 Mouse anti-NeuN	Abcam, ab104224
	1:200 Sheep anti-PV	SWANT, PV235
	1:500 Rabbit anti-CR	Abcam, ab702
CONDITION 2	1:1000 Mouse anti-NeuN	Abcam, ab104224
	1:200 Sheep anti-PV	SWANT, PV235
	1:1000 Rabbit anti-CB	SWANT, CB-38

Table 1. Sources and concentrations of primary antibodies. Combinations of antibodies in each experimental antibody condition for immunohistochemistry is shown.

Area V1
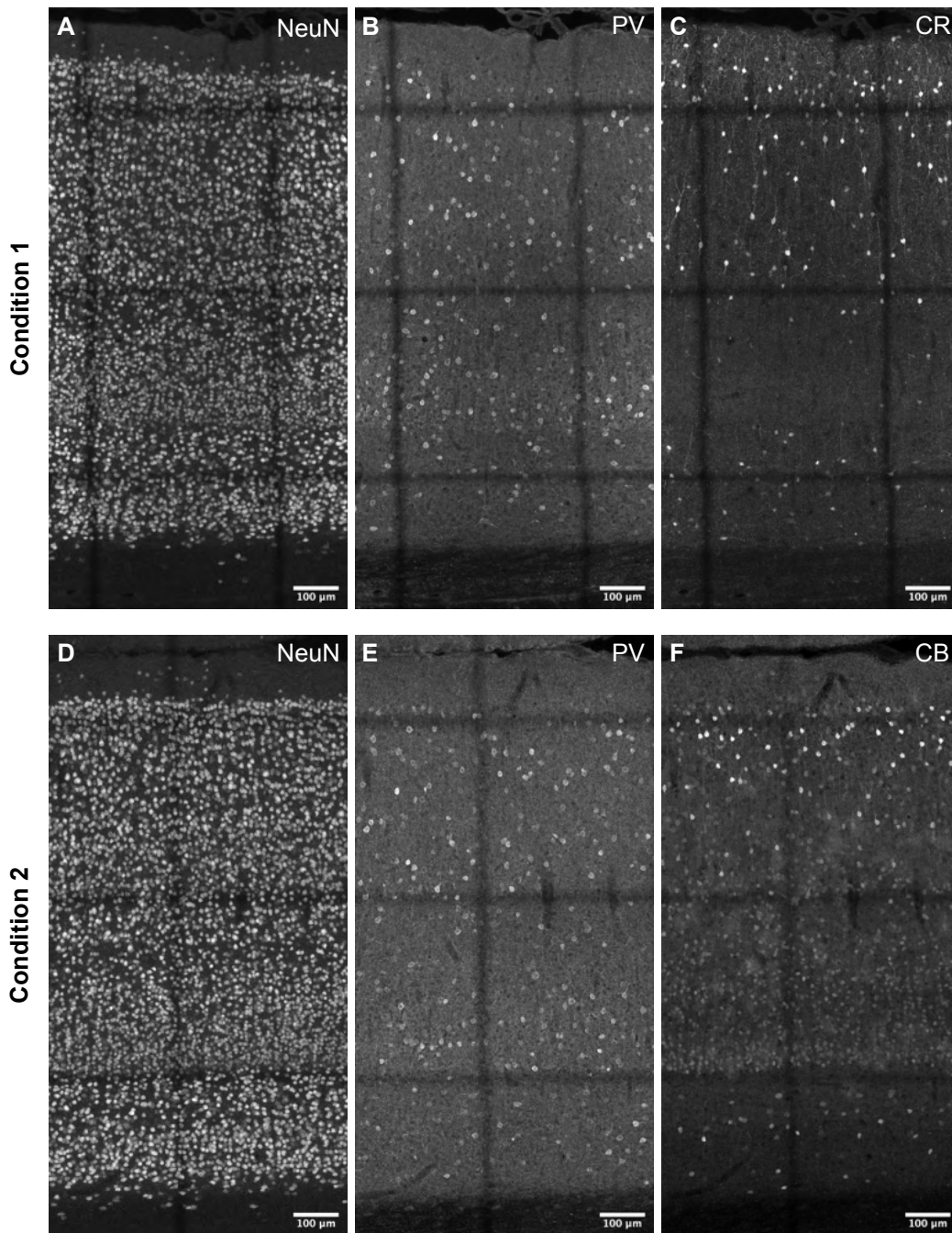
Figure 3. Maximum intensity images of each staining condition used. Sample images shown from marmoset primary visual cortex. (**A-C**) Antibody staining condition 1 containing NeuN, anti-PV, and anti-CR antibodies. (**D-F**) Antibody staining condition 2 containing NeuN, anti-PV, and anti-CB antibodies.

2.4 Image acquisition and counting window

Z-stack images were acquired using a Leica SP8 confocal microscope with a z-step size of 0.4 µm at 20X magnification and imported to imageJ software for manual cell counting and analysis. The focus map feature in Leica software was used to set a different starting z-position for each tile within an acquisition.

Using the region of interest (ROI) manager tool in imageJ, a 700- µm-wide polygonal counting window spanning pia to white matter was drawn over the area of interest (Fig. 4A, B), as identified by the Marmoset Brain Atlas and the Marmoset Gene Atlas database (Paxinos et al., 2012; Shimogori et al., 2018). Cortical layers boundaries were identified by assessing cell and neuron distributions in the DAPI and NeuN channels, respectively. In addition, known layer-specific gene markers (Mashiko et al., 2012) were cross-referenced with the Marmoset Gene Atlas database to guide identification of cortical layer boundaries (Shimogori et al., 2018).

2.5 Manual cell counting and antibody penetration depth

Cells were manually counted using the Cell Counter plugin in imageJ. Markers were placed at the center of each cell in the z-plane in which the soma appeared the brightest. Cell counts were performed based on their immunoreactivity. Cells that were CB-immunoreactive appeared to have two distinct subpopulations based on their staining intensity: a high-intensity group and a low-intensity group. This characteristic of CB-immunoreactive cells has been observed in past studies (Bourne et al., 2007; Kooijmans et al., 2020). It is thought that the low-intensity group exhibits excitatory properties, therefore we have opted to exclude this subpopulation from our cell counts (Van Brederode, Mulligan, & Hendrickson, 1990). We accomplished this by first measuring background

intensity within the tissue. We then multiplied the background intensity value by 2.5 and subtracted the resulting value from the acquisition's overall intensity. This method was determined empirically through trial and error to determine the optimal subtract value that would filter out low-intensity CB cells while preserving high-intensity CB cells.

Cell bodies that made contact with any side of the counting window boundary were excluded. In imageJ, the "Plot Z-axis Profile" tool was used on a square area of roughly 150 µm x 150 µm to evaluate signal intensity throughout the image stack's depth. The area to be sampled was selected at random and was ensured to contain cell bodies. The resulting plot showed signal intensity along throughout the imaged tissue depth and was used to determine antibody penetration depths. The penetration depth was defined as the depth range at which maximum signal intensity occurred to the depth at which 80% of maximum signal intensity occurred. Determining each antibody's penetration profile ensures that there is sufficient and consistent signal intensity throughout the entire counting volume. This process was repeated for each of the three interneuron antibodies used in this study. The penetration depths were determined to be 4.05 µm, 7.00 µm, and 7.30 µm for PV, CB, and CR antibodies, respectively.

2.6 *MATLAB cell count analysis*

The coordinates for layer ROIs and counted cells were exported from imageJ as an excel document and imported to MATLAB for analysis. A MATLAB script was first generated to organize cell counts based on cell types, then by cell density per layer based on both cell count coordinates and layer ROI coordinates. Antibody penetration depths were incorporated into the script to filter out cells that fell outside of the counting depth

ranges. Individual cell densities acquired from each tissue sample and from each animal subject are reported in Figure 15.

2.7 Cell densities and proportions

Total interneuron densities were reported as number of cells per cubic millimeter and were calculated by dividing the number of cells by the overall counting volume. Layer-wise interneuron densities were also calculated by dividing the number of cells within a given cortical layer by the volume of the given cortical layer. This calculation was performed individually for each image stack.
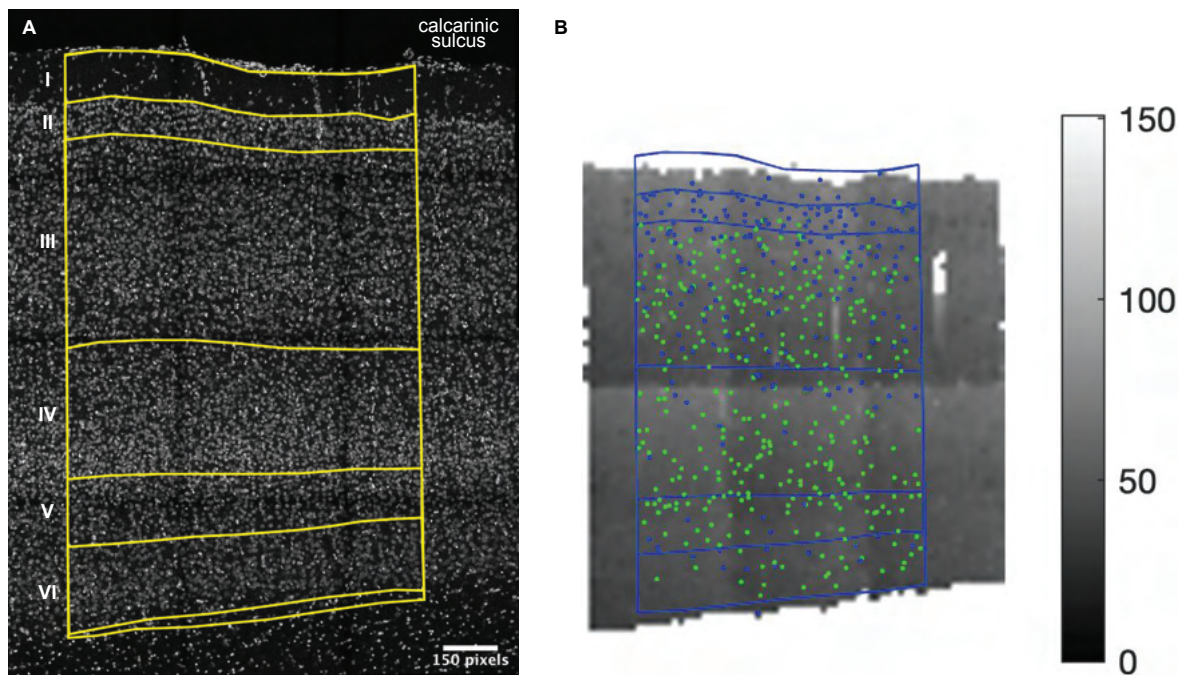
Figure 4. Sample cell counting window from V1 tissue with layer boundaries and respective surface map. (**A**) Counting window and layer boundary overlay in the DAPI channel. Counting window and layer border overlay created using ROI Manager in imageJ software. (**B**) Surface map of tissue generated in imageJ software and used to determine z-position of tissue surface.

The abundance of each interneuron was reported both as layer-wise and total interneuron density (Table 3). The densities of each interneuron subtype were also normalized to total interneuron density for a given area (Fig. 9). This was done by dividing the absolute density of a given interneuron by the sum of all three interneuron densities within a given cortical area.

Layer-wise normalization was also performed for each interneuron subtype in each of the cortical areas. This was done by dividing the density of a given interneuron in a given cortical layer by the total density of that interneuron across all layers in the cortical area of interest.

$$Normalized\ total\ PV_{V1} = \frac{PV_{V1}}{PV_{V1} + CB_{V1} + CR_{V1}}$$

Formula 1. Sample calculation of total interneuron density normalization for PV cells in V1. Subscripts indicate the cortical area that the density data originates from.

$$Normalized\ layer-wise\ density\ PV_{L1,V1} = \frac{PV_{L1,V1}}{Total\ PV_{V1}}$$

Formula 2. Sample calculation of layer-wise interneuron density normalization for PV cells in cortical layer 1 (L1) of V1. Subscripts indicate the cortical layer and cortical area that the density data originates from.

2.8 Colocalization of calcium-binding protein markers

Colocalization of PV, CB, and CR interneurons was assessed to ensure that observations throughout the study are not misrepresented due to cross-reactivity of

markers. Past studies have reported colocalization between PV and CB markers and between PV and CR markers in marmoset, macaque, and human models, therefore, PV/CB and PV/CR colocalization was analyzed (Hendry et al., 1989; Van Brederode et al., 1990; Meskenaite et al., 1997; Leuba et al., 1998). Colocalization values are represented as the proportion of a cell type that colocalizes with another given calcium-binding protein marker.

2.9 Direct comparison to past findings

The data from the study by Torres-Gomez et al. (2020) was reworked to eliminate NG cell counts and allow for interneurons abundance to be represented as a proportion of total interneurons rather than total neurons. This was done by saving the data figure (Fig. 2) as a '.jpg' formatted image and importing it into Fiji software. The measure tool was used to measure the height of each bar in the graph for all markers except NG. The values of the measurement correspond to the mean percentage value corresponding to each interneuron as its proportion of total neurons, as indicated on the y-axis label of the original graph. Three measurements were collected for each bar in the graph and the mean of those three measurements were used to account for human error during the measurement of each bar's height.

Once all measurements were collected, the measures from each cortical area were summed. This resulted in a sum of PV, CB, and CR percentages for each of the three cortical areas; MT, MST, and LPFC. The calculation shown in Equation 1 was performed for each interneuron subtype in each cortical area. By excluding NG from this calculation, we were able to determine the abundance of each interneuron as a proportion of total

interneurons rather than a proportion of total neurons, allowing for a direct comparison between the results of Torres-Gomez and the results of the current study.

2.10   Overall project organization

The brains of two male marmosets were used in this study and 18 tissue sections were collected from each animal, resulting in a total of 36 tissue sections combined. The 18 sections per animal were comprised of six sections from each of the three areas of interest, which allowed us to acquire three counts per cell type per area in each animal. Two sections from each animal had to be discarded due to damages to the tissue that interfered with counting. As a result, we gathered a total of 32 counts (16 per animal).

Cortical area	Interneuron cell type	Number of counts acquired
	CB	5
V1	CR	5
	PV	6
	CB	5
LIP	CR	6
	PV	6
	CB	5
PFC	CR	6
	PV	6

Table 2. Total number of cell counts acquired per cortical area and interneuron cell type.

2.11   Statistical analysis

Statistical analysis was performed using number of tissue sections as n values, as reported in Table 2. A two-way ANOVA was performed to assess the differences in the densities of interneuron subtypes across cortical areas and across cortical layers. A Tukey-Kramer post-hoc analysis was subsequently performed to assess individual differences. All

statistical analysis was completed in MATLAB R2021a software, and all values are represented as mean ± standard deviation, where applicable.

The *n* value used in statistical analyses throughout the current study represents number of tissue sections rather than number of animal subjects. The *n* value is defined as the number experimental units for each condition and, therefore, the number of independent observations. Each tissue section is deemed to be an independent observation on the basis that each tissue section stained separately but under identical staining conditions and consistent staining protocols, imaged separately but with identical imaging parameters, and underwent identical image processing until it was ultimately followed by subjective manual counting.

3 – Results

3.1 Cross-area comparisons of inhibitory interneurons

The current study considers the past study by Torres-Gomez et al. (2020) as both a point of direct comparison for the current study due to the high level of methodological similarities, and as the foundational work for the current study to elaborate upon. For this reason, the current study has made an adjustment to the original figure from Torres-Gomez et al. (2020) to derive an alternate representation of the same results but in a way that better facilitates direct comparison to our results. This adjustment was made by eliminating neurogranin (NG) from the original data to represent interneurons proportions as percentages of total interneurons rather than total neurons, as we have not included a total neuron count in the current study.

3.1.1 Cross-area comparison of interneuron densities

The abundance of each interneuron subtype was compared across cortical areas V1, LIP, and PFC. Interneuron abundance was represented as the proportion of total interneurons, as per equation 1, converted into a percentage. Our findings uncovered a main effect by cortical area on PV (n=17, $F_{(2, 48)} = 6.16$, $P = 1.2028e-2$) with a significant decrease in PV proportion from V1 to PFC ($P = 9.6355e-3$). PV interneurons were found to make up approximately 64.35% of total interneurons in V1 and 37.16% of total interneurons in PFC. Although there appears to be a decreasing trend in the proportion of PV from V1 to LIP as well, this difference was not found to be significant ($P = 0.090984$). PV was found to make up approximately 46.48% of the total interneuron population in LIP. No significant difference was found between PV proportions of LIP and PFC (Fig. 6).

23

In addition, we found a main effect by cortical area on CR proportions (n=17, $F_{(2, 48)}$ = 35.01, P = 3.5680e-6). We observed a significant increase in the proportion of CR from V1 to LIP (P = 8.3056e-5) and from V1 to PFC (P = 3.1430e-6). CR was found to make up approximately 18.14% of total interneurons in V1, 34.49% of those in LIP, and 40.14% of those in PFC.

No significant difference was found between the CR proportions of LIP and PFC (Fig. 6).

No significant differences were found in the proportions of CB between any of the cortical areas of interest, however, a non-significant increasing trend was observed from V1 to LIP to PFC. Approximately 17.51% of V1 interneurons, 19.02% of LIP interneurons, and 22.69% of PFC interneurons were found to be CB (Fig. 6).

3.1.2   *Adjusted representation of Torres-Gomez results*

Each interneuron subtype is represented as a percentage of total interneurons in cortical layers II/III for each cortical area using data derived from Torres-Gomez et al. (2020) (Fig. 6B). This adjusted representation shows that PV cells make up 30%, 29.32%, and 24.37% of total interneurons in MT, MST, and LPFC, respectively (Fig. 6B). The original data indicated a significant main effect by cortical area on PV cells with a significant decrease from MT to LPFC, and from MST to LPFC (Fig. 6A).

CB cells were found to make up 27.68%, 27.53%, and 26.84% of inhibitory interneurons in MT, MST, and LPFC respectively in this adjusted representation (Fig. 6B). The original data uncovered no significant main effect by cortical area on CB cells (Fig. 6A).

CR cells were found to make up 42.32%, 43.15%, and 48.79% of inhibitory interneurons in MT, MST, and LPFC, respectively (Fig. 6B). The original data indicated a

significant main effect by cortical area on CR with a significant increase in CR percentage

from MT to LPFC, and from MST to LPFC (Fig. 6A).
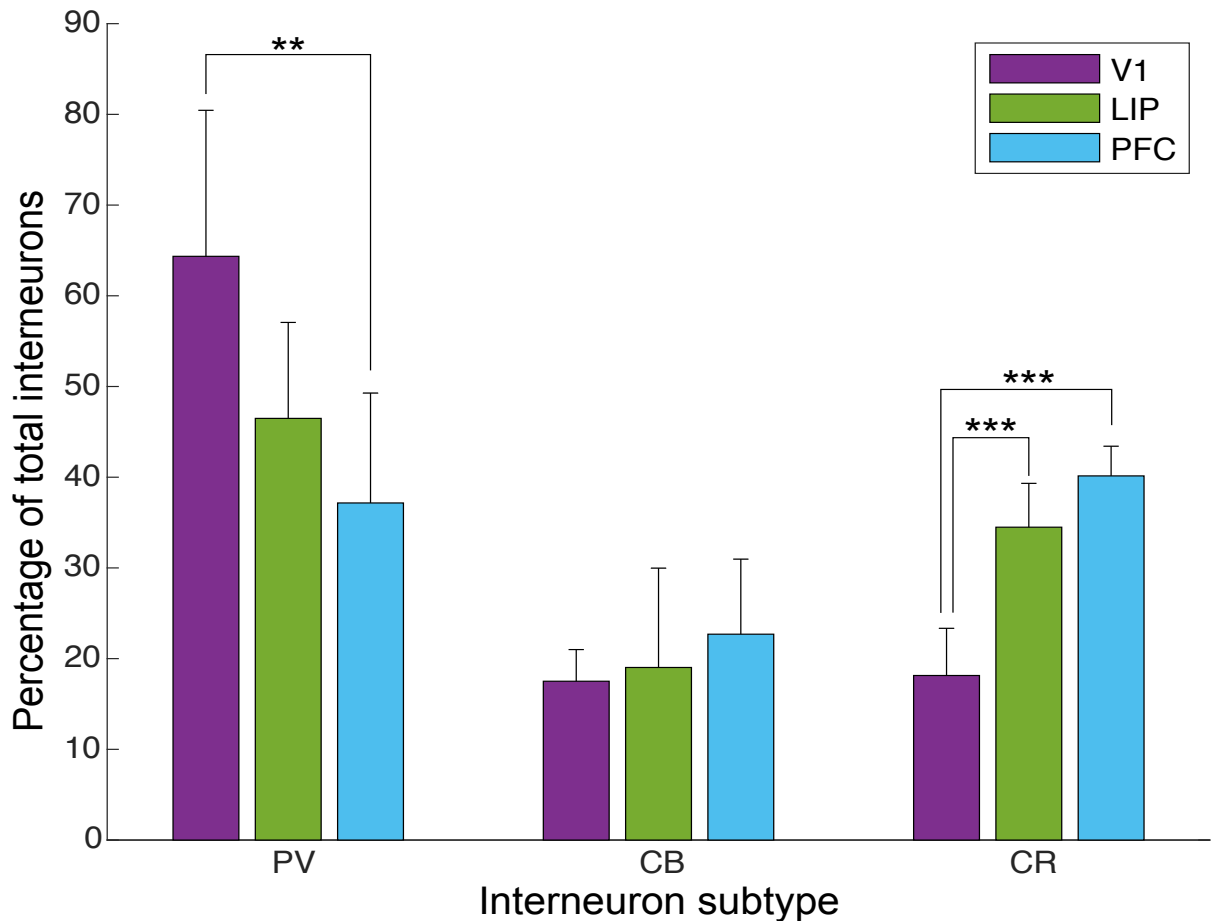
Figure 5. Cross-area comparison of PV, CB, and CR abundance as percentages of total interneurons for cortical areas V1, LIP, and PFC. Asterisks represent significance differences. Double asterisks represent $p \leq 0.01$. Triple asterisks represent $p \leq 0.001$. All values shown as mean ± standard deviation.

3.1.3 Direct comparison of findings to Torres-Gomez et al. (2020)

The results of the current study are in alignment with the findings of Torres-Gomez et al. (2020) with respect to relative interneuron abundance across sensory and association areas; both results demonstrate a decrease in PV proportions, an increase in CR proportions, and no changes in CB proportions as we approach cortical area PFC from early sensory areas (Fig. 5, 6).
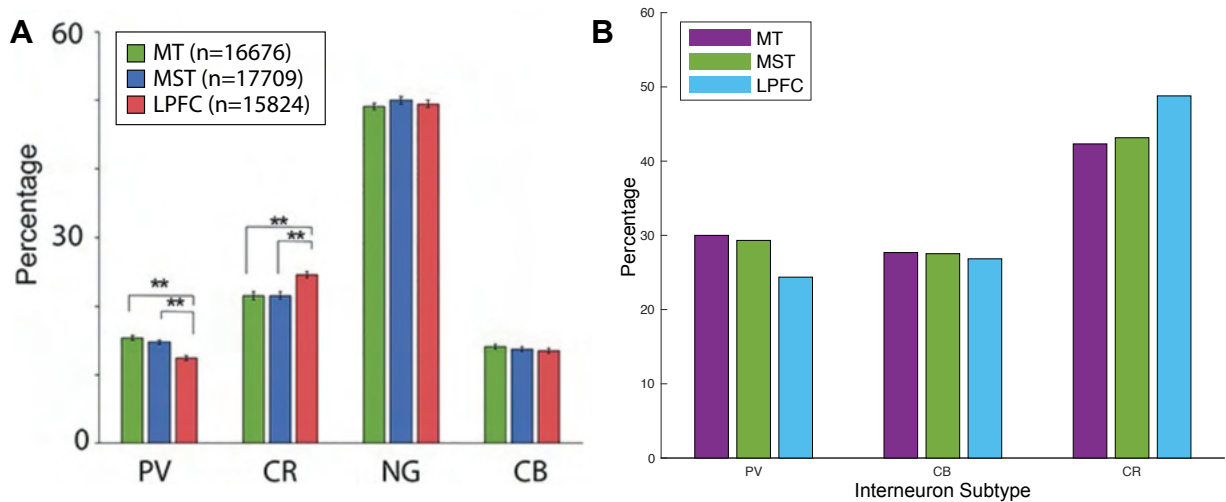
Figure 6. Original and adjusted representation of interneuron proportion results from past study. Abundance of PV, CR, NG, and CB in layer II/III is shown as a percentage of total neurons across areas MT, MST, and LPFC (**A**). NG was removed from original data to represent PV, CB, and CR as percentage of total interneurons across MT, MST, and LPFC (**B**). All data derived from Torres-Gomez et al. (2020). All values shown as mean ± standard deviation.

There are differences between the two studies with respect to the absolute proportions of individual interneurons. Although the statistical data is not available for comparisons between the two studies, there is a pattern of lower relative PV density in the study by Torres-Gomez et al. when compared with the current study. Additionally, there is a pattern of higher relative CB and CR densities in the study by Torres-Gomez et al. when compared with the current study (Table 3).

	Torres-Gomez et al.			Current Study		
	MT	MST	PFC	V1	LIP	PFC
PV	30.00	29.32	24.37	64.35 ± 16.10	46.49 ± 10.58	37.16 ± 12.12
CB	27.68	27.53	26.84	17.51 ± 3.49	19.02 ± 10.96	22.69 ± 8.28
CR	42.32	43.15	48.79	18.14 ± 5.20	34.49 ± 4.83	40.14 ± 3.28

Table 3. Comparison of interneuron abundances as percentages of total interneurons across two studies. Findings from a past study by Torres-Gomez et al. (2020) is shown alongside the findings from the current study. Both studies analyzed the same three inhibitory interneurons; PV, CB, and CR. Torres-Gomez et al. analyzed interneuron abundance in cortical areas MT, MST, and PFC while the current study analyzed interneuron abundance in cortical areas V1, LIP, and PFC. All values shown represent percentages of total interneurons for a given cortical area. Values shown as mean ± standard deviation. Standard deviation values not available for data derived from Torres-Gomez et al. study.

3.2 Laminar distribution of interneurons across cortical areas

Each interneuron subtype has a characteristic spatial distribution across cortical layers, meaning that interneurons are not evenly distributed across all cortical layers. This study has expanded upon the findings of its cross-area comparison and the findings of Torres-Gomez et al. (2020) by exploring the laminar distribution of each interneuron subtype across all cortical layers and all cortical areas of interest.

Initial qualitative and quantitative assessments of laminar distributions for each interneuron subtype in each cortical area was performed as a quality control check to ensure that the immunohistochemical markers used were truly representing the intended subpopulations of INs based on their characteristic laminar distributions. The immunostainings confirmed that the laminar distribution observed of each interneuron subtype is consistent with findings of past studies (Goodchild and Martin, 1998; Hof et al., 1998; Bourne et al., 2007). Parvalbumin interneurons appear to be the most abundant of all three cell types and are present throughout all layers. Parvalbumin cells were found to be most abundant in layers III-V with relatively lower density in layer I (Fig. 7B, 8B, 9B, Table 4). These observations are consistent with past findings characterizing the laminar distribution of PV interneurons (Van Brederode et al., 1990; DeFelipe et al., 1999). Calretinin interneurons are present in all layers and have highest density in layer II (Fig. 7C, 8C, 9C, Table 5), which also agrees with the findings of past studies (Hof et al., 1998). Calbindin interneurons appear to have high-intensity and low-intensity subpopulations, as expected (Fig. 7E, 8E. 9E) (Goodchild and Martin, 1998; Bourne et al., 2007; Kooijmans et al., 2020). Only the high-intensity subpopulation was included in our counts and was found to have the highest density in layers II and III as reported by past studies (Fig. 7E,

8E, 9E, Table 6) (Goodchild and Martin, 1998; Hof et al., 1998, Bourne et al., 2007). The

laminar profiles of each of the inhibitory interneuron subtypes were found to be consistent

across all three cortical areas (Table 4).

Figure 7. Maximum projection images displaying laminar distributions of interneuron subtypes in V1. Laminar boundaries identified using NeuN maximum projects from antibody condition 1 (**A**) and antibody condition 2 (**D**) as references. Laminar distributions of PV (**B**), CR (**C**) and CB (**E**) are shown.

Area LIP
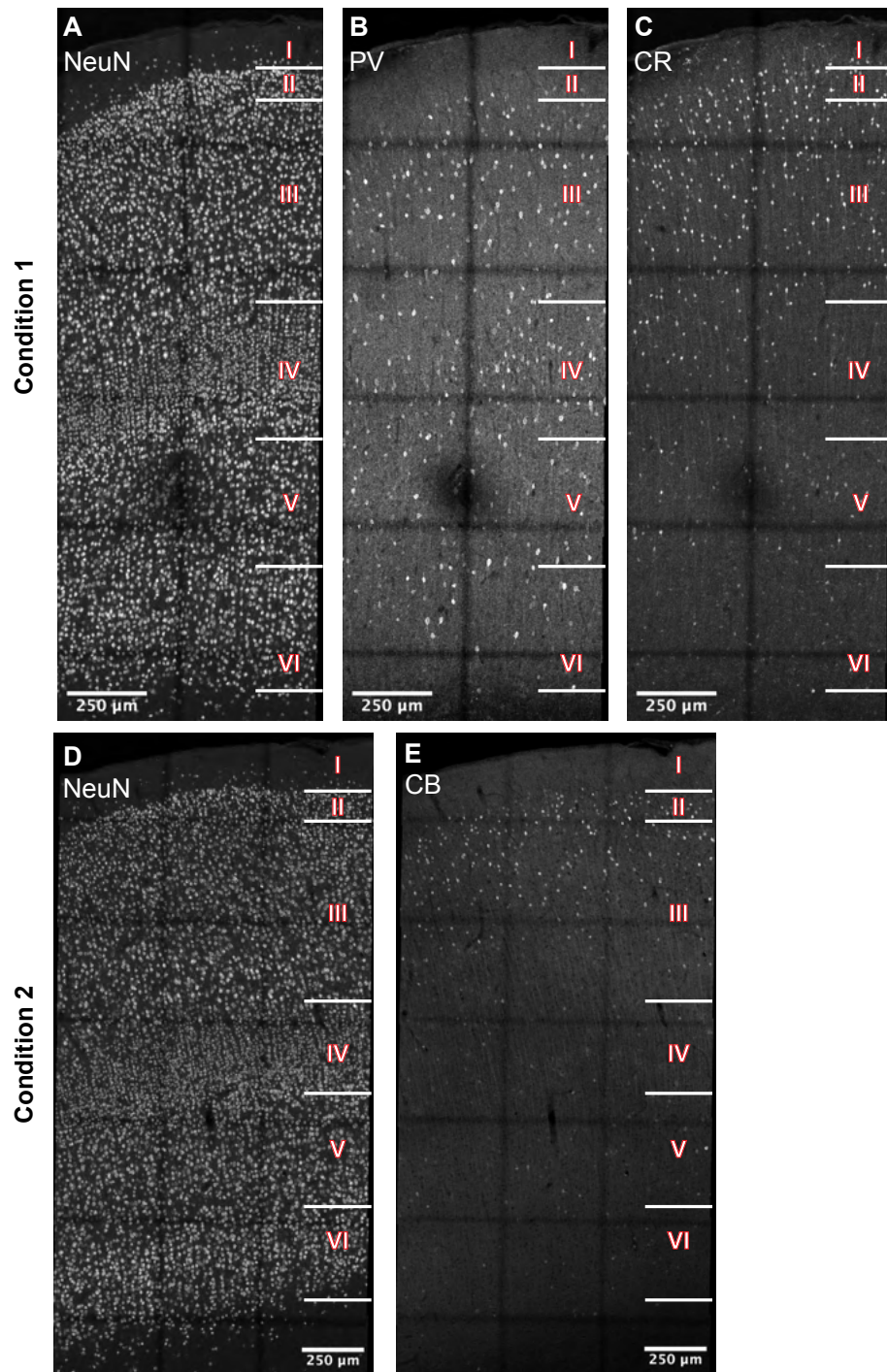
Figure 8. Maximum projection images displaying laminar distributions of interneuron subtypes in LIP. Laminar boundaries identified using NeuN maximum projects from antibody condition 1 (**A**) and antibody condition 2 (**D**) as references. Laminar distributions of PV (**B**), CR (**C**) and CB (**E**) are shown.
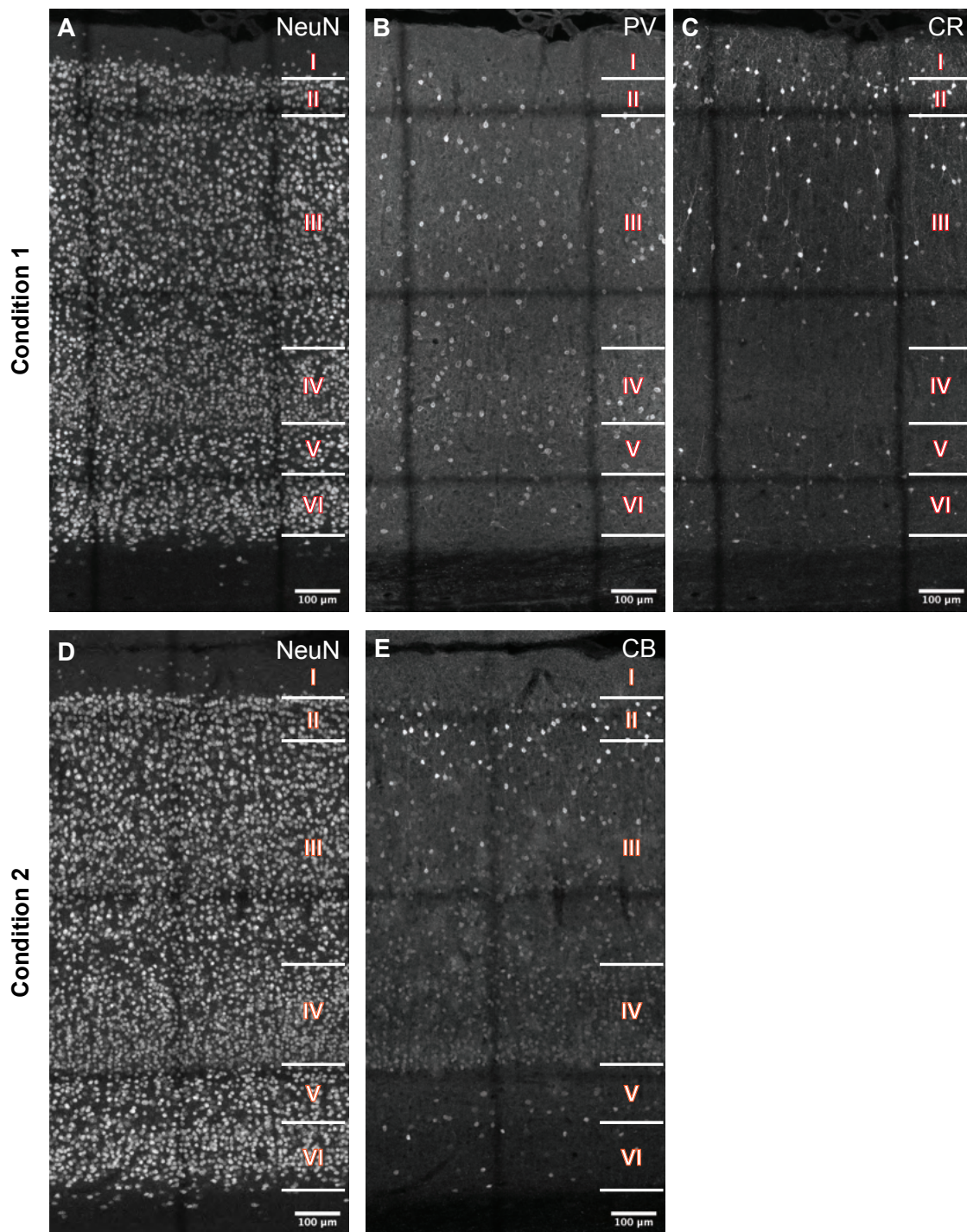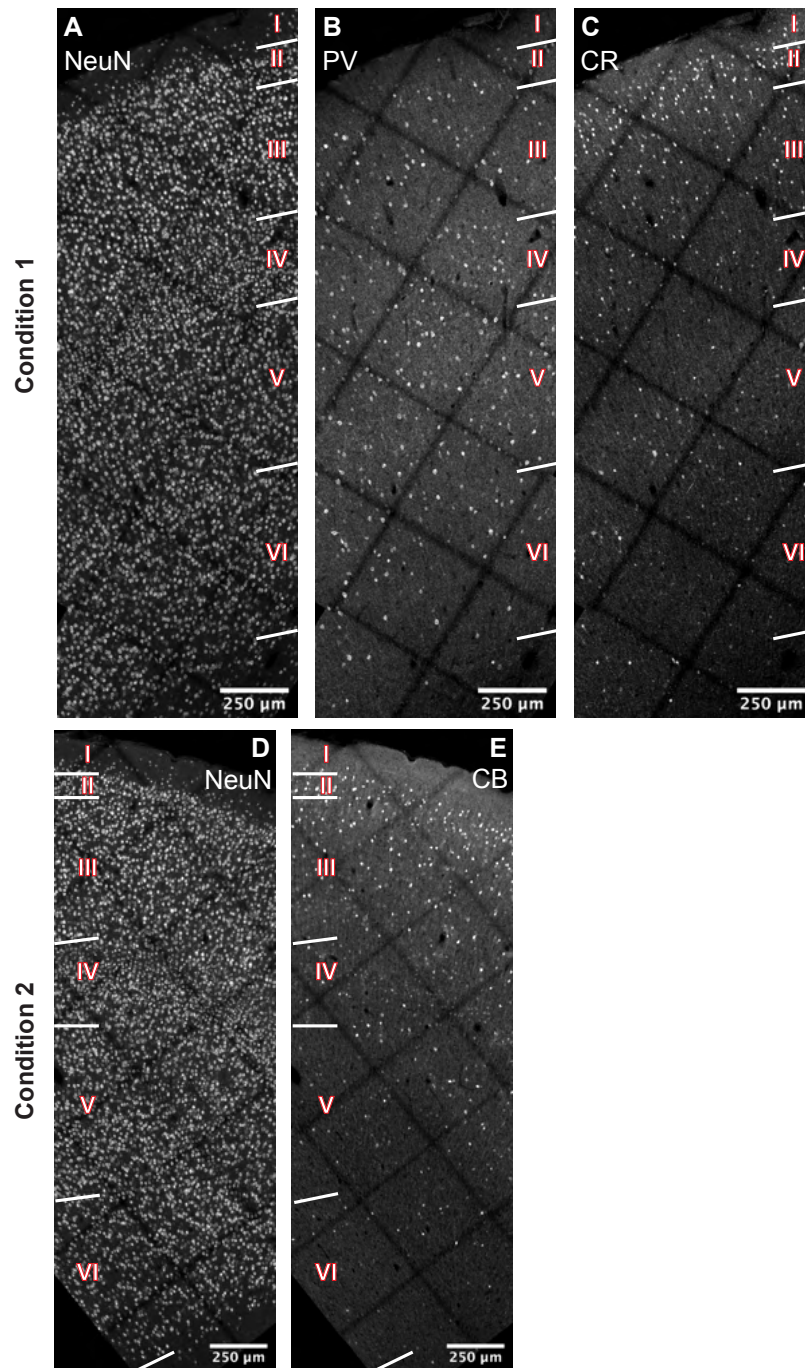
Figure 9. Maximum projection images displaying laminar distributions of interneuron subtypes in PFC. Laminar boundaries identified using NeuN maximum projects from antibody condition 1 (**A**) and antibody condition 2 (**D**) as references. Laminar distributions of PV (**B**), CR (**C**) and CB (**E**) are shown.

	V1	LIP	PFC
L1	0	0.0145 ± 0.0356	0.2179 ± 0.2683
L2	0.5134 ± 0.4270	0.8024 ± 0.4215	0.8398 ± 0.7422
L3	1.4160 ± 0.5102	0.9614 ± 0.1694	1.4523 ± 0.6841
L4	1.7402 ± 0.4767	1.9216 ± 0.2752	1.6333 ± 0.3859
L5	1.3655 ± 0.7260	1.1394 ± 0.3157	0.8542 ± 0.4231
L6	0.6712 ± 0.1609	0.6415 ± 0.1000	0.3944 ± 0.2590

Table 4. Layer-wise PV density across cortical areas normalized to total PV density of each cortical area. Values represent proportion of PV density of a given layer to the total PV density of the given cortical area. Values represented as mean ± standard deviation.

3.2.1 Spatial distribution of parvalbumin interneurons

Parvalbumin's overall spatial distribution is similar across all three cortical areas with no significant interaction effect found between cortical area and cortical layer for normalized PV proportions (n = 17 total tissue sections, $F_{(10,84)} = 1.41$, P = 0.19) (Fig. 10, Table 4).

There is a main effect by cortical layer on normalized PV proportion (n = 17 total tissue sections, $F_{(5,84)} = 33.78$, P = 0). There is a significantly greater proportion of PV in layer IV compared with all other cortical layers with its mean PV proportion of 1.7665 ± 0.2085; the proportion of PV in layer IV is significantly greater than that of adjacent cortical layer III (P = 0.0122) and significantly less than that of adjacent cortical layer V (P = 2.9004e-4). This laminar distribution for PV interneurons is consistent with the findings of past studies indicating that PV is most abundant in cortical layer IV (Van Brederode et al., 1990; DeFelipe et al., 1999; Goodchild and Martin, 1998; Hof et al., 1998; Bourne et al., 2007).

Figure 10. Normalized spatial distribution of PV interneurons across cortical areas. Maximum projection of PV-immunoreactive cells in V1 (**A**), LIP (**B**), and PFC (**C**). Normalized layer-wise abundance of PV interneurons across cortical areas. PV density of each layer is normalized to the total PV density of all layers for a given cortical area (**D**). All values shown as mean ± standard deviation.

3.2.2   Spatial distribution of calretinin interneurons

	V1	LIP	PFC
L1	0.9240 ± 0.7610	0.9195 ± 0.2223	1.0444 ± 0.6917
L2	4.7774 ± 1.6899	3.3786 ± 0.2688	2.9329 ± 0.6726
L3	1.4885 ± 0.4442	1.5343 ± 0.1631	1.3284 ± 0.2486
L4	0.4637 ± 0.1818	0.4989 ± 0.1392	0.7350 ± 0.2039
L5	0.7268 ± 0.8059	0.5229 ± 0.0669	0.6116 ± 0.2241
L6	0.7148 ± 0.2230	0.1561 ± 0.1038	0.3399 ± 0.1221

Table 5. Layer-wise CR density across cortical areas normalized to total CR density of each cortical area. Values represent proportion of CR density of a given layer to the total CR density of the given cortical area. Values represented as mean ± standard deviation. as mean ± standard deviation.

A two-way ANOVA revealed a significant interaction effect between cortical layer and cortical area with respect to normalized CR proportions (n = 17 total tissue sections, $F_{(10,84)} = 2.98$, P = 0.0029).

Furthermore, there is a significant main effect by cortical layer on normalized CR proportion (n = 17 total tissue sections, $F_{(5,84)} = 89.79$, P = 0). There is a significantly greater mean normalized proportion of CR in cortical layer II compared with all other cortical layers. The mean normalized CR proportion of cortical layer II is 3.6960 ± 0.2702, which is significantly greater than that of its adjacent cortical layers I (P = 3.8576e-24) and III (P = 4.3202e-19) (Fig. 11, Table 5). This laminar distribution for CR interneurons is consistent with the findings of past studies (Hof et al., 1998).

In addition, there a two-way ANOVA revealed a significant main effect by cortical area on mean normalized CR proportion (n = 17 total tissue sections, $F_{(2, 84)} = 3.85$, P = 0.0251). There is a significantly higher proportion of CR interneurons localized to layer II in V1 compared with LIP (P = 0.0500) and in V1 compared with PFC (P = 0.0449).
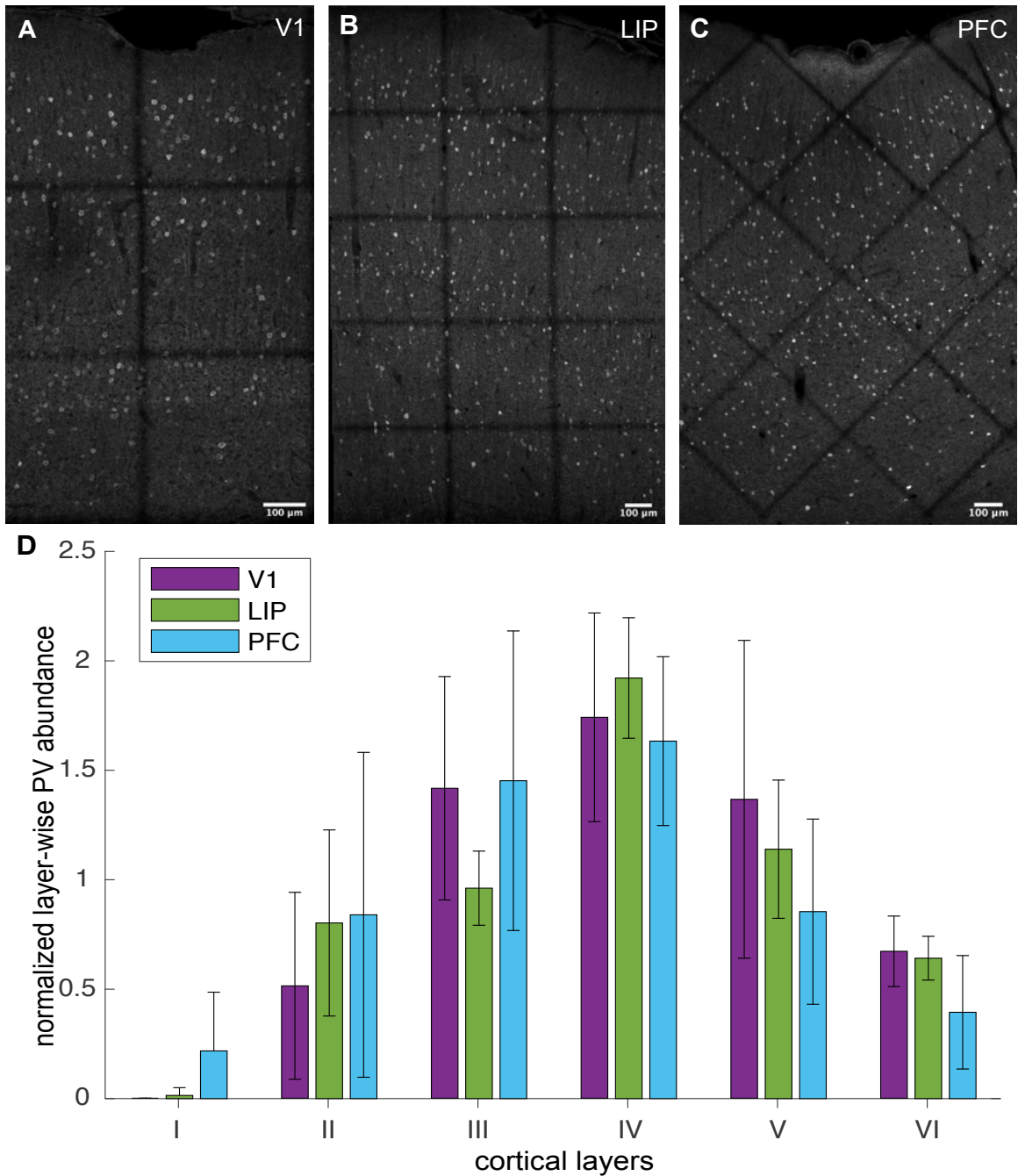
Figure 11. Normalized spatial distribution of CR interneurons across cortical areas. Maximum projection of CR-immunoreactive cells in V1 (**A**), LIP (**B**), and PFC (**C**). Normalized layer-wise abundance of CR interneurons across cortical areas. CR density of each layer is normalized to the total CR density of all layers for a given cortical area (**D**). All values shown as mean ± standard deviation.

3.2.3 Spatial distribution of calbindin interneurons

	V1	LIP	PFC
L1	0.0901 ± 0.1248	0.1208 ± 0.1284	0.1185 ± 0.1218
L2	3.502 ± 0.7126	4.3208 ± 0.8645	3.3742 ± 1.7734
L3	1.355 ± 0.2260	1.8019 ± 0.1777	1.7495 ± 0.7286
L4	0.7619 ± 0.4592	0.1557 ± 0.1737	0.5172 ± 0.3597
L5	0.2298 ± 0.1817	0.1998 ± 0.1159	0.4337 ± 0.2578
L6	0.2210 ± 0.1976	0.0952 ± 0.1238	0.1448 ± 0.1568

Table 6. Layer-wise CB density across cortical areas normalized to total CB density of each cortical area. Values represent proportion of CB density of a given layer to the total CB density of the given cortical area. Values represented as mean ± standard deviation.

Calbindin's overall spatial distribution is similar across all three cortical areas with no significant interaction effect found between cortical area and cortical layer for normalized CB proportions (n=15 total tissue sections, $F(10,72) = 1.36$, $P = 0.22$) (Fig. 12, Table 6).

There is a main effect by cortical layer on normalized CB proportion (n = 15 total tissue sections, $F(5,72) = 97.27$, $P = 0$). There is a significantly greater proportion of CB in cortical layer II followed by cortical layer III compared with all other layers. The mean normalized CB proportion of cortical layer II is 3.7322 ± 0.2988, which is significantly greater than that of its adjacent cortical layers I ($P = 1.1766e-27$) and III ($P = 1.2744e-14$). The mean normalized CB proportion of cortical layer III is 1.6356 ± 0.2988, which is significantly higher than that of its adjacent cortical layer IV ($P = 4.0474e-6$). This laminar distribution for CB interneurons is consistent with the findings of past studies indicating that CB is most abundant in cortical layers II/III (Goodchild and Martin, 1998; Hof et al., 1998, Bourne et al., 2007).
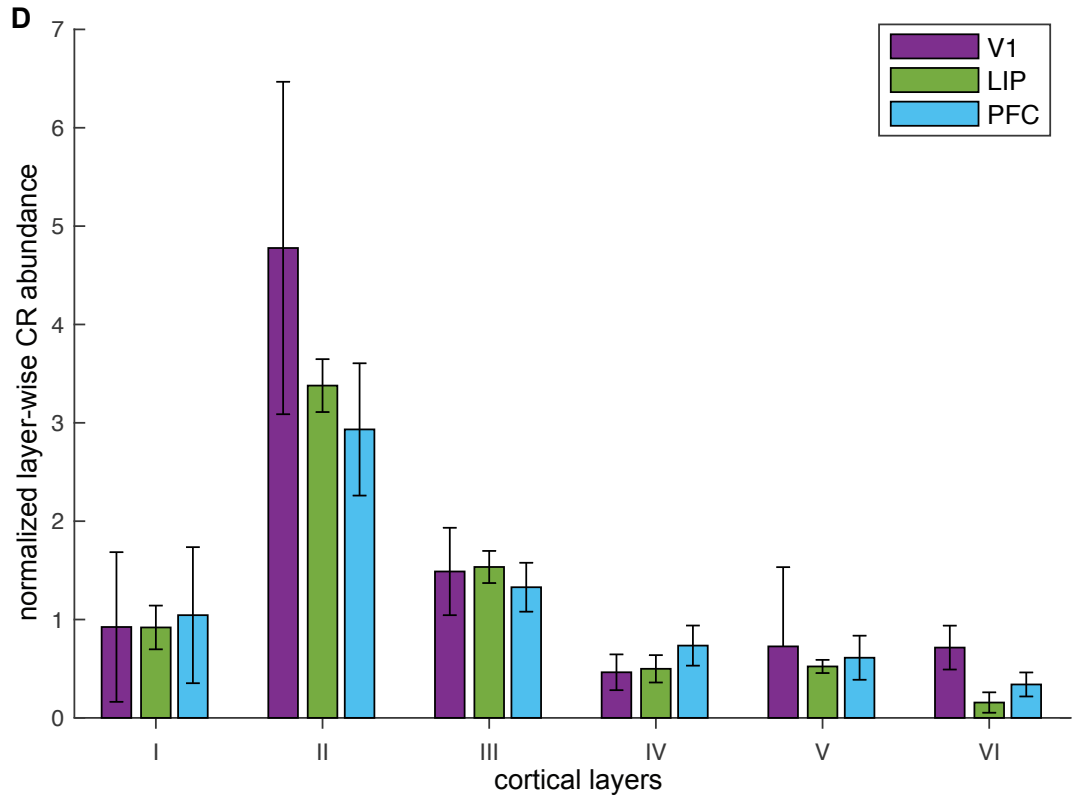
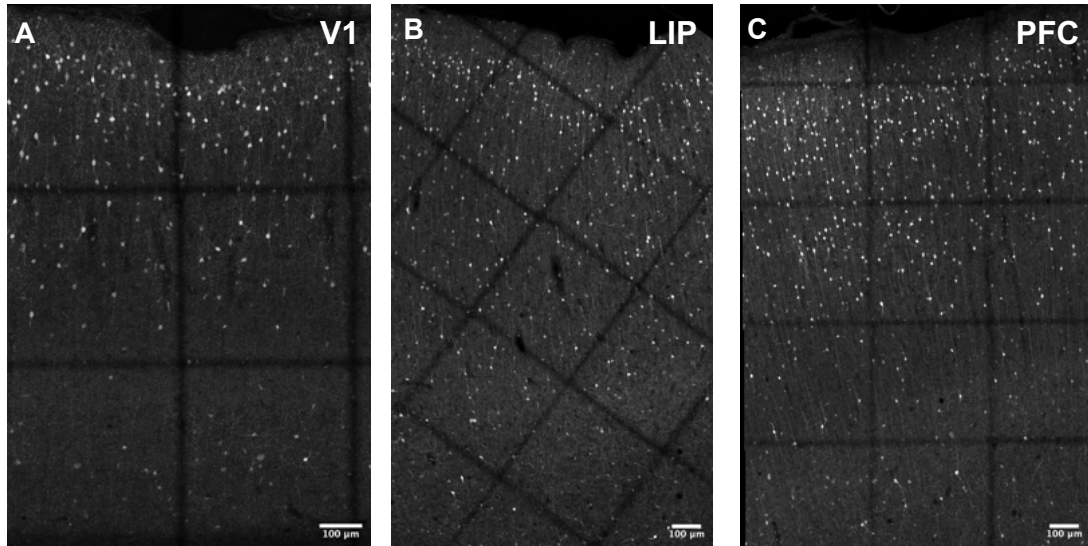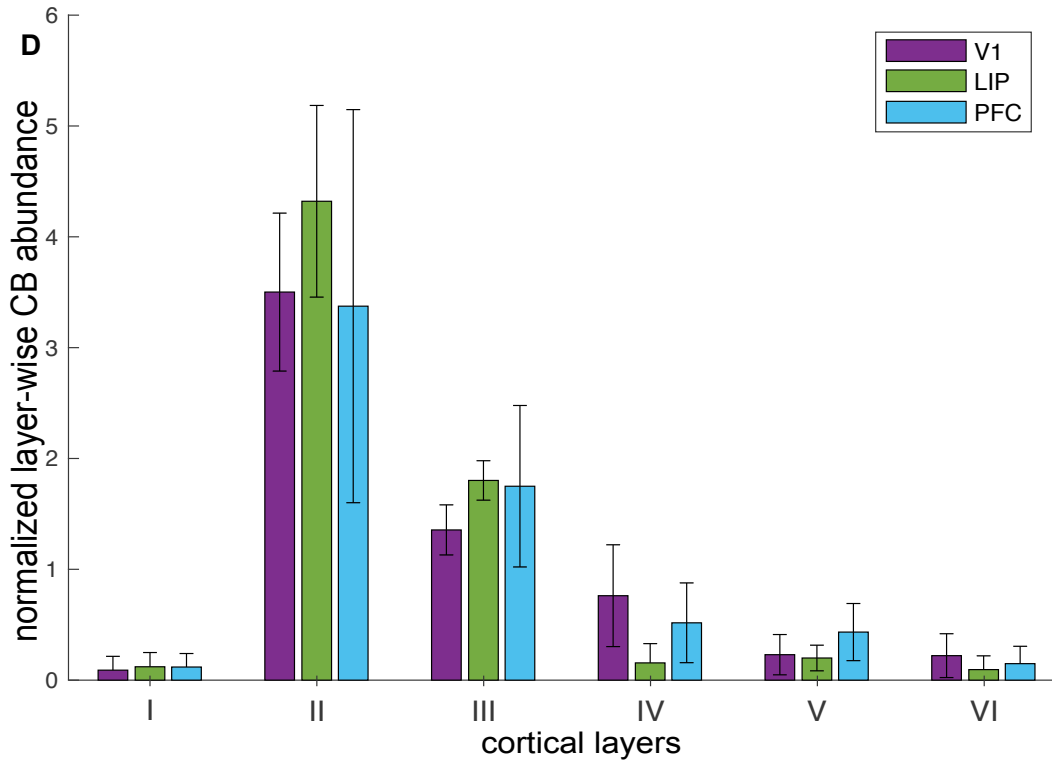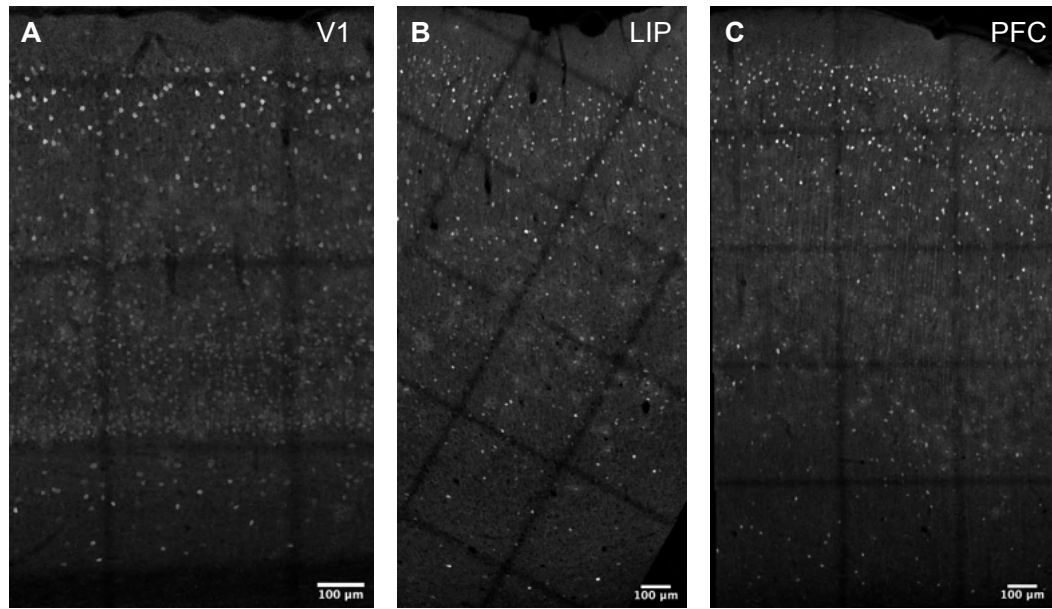**Figure 12.** Normalized spatial distribution of CB interneurons across cortical areas. Maximum projection of CB-immunoreactive cells in V1 (**A**), LIP (**B**), and PFC (**C**). Normalized layer-wise abundance of CB interneurons across cortical areas. CB density of each layer is normalized to the total CB density of all layers for a given cortical area. (**D**). All values shown as mean ± standard deviation.

3.3 Colocalization of Inhibitory Interneuron Markers

Previous studies have shown little to no overlap between PV, CB, and CR interneuron markers and they are therefore believed to represent non-overlapping populations of inhibitory interneurons (DeFelipe, 1997). Several primate studies, however, have reported low levels of colocalization between PV and CB markers and between PV and CR markers in marmoset, macaque, and human models (Hendry et al., 1989; Van Brederode et al., 1990; Meskenaite et al., 1997; Leuba et al., 1998). Our observations of colocalization between PV and CB markers and between PV and CR markers are in alignment with reports from past studies.

3.3.1 Colocalization of PV/CB

A low level of colocalization was observed between PV and CB interneurons. Approximately 4.6%, 2.1% and 5.0% of PV cells and 9.5%, 5.0%, and 10.4% of CB cells colocalized with one another in V1, LIP, and PFC, respectively (Fig. 13A). Overall, colocalization levels remained at an approximate proportion of 10% or less and were therefore determined to be negligible in the current study's assessment of total interneuron densities across cortical areas.

3.3.2 Colocalization of PV/CR

A low level of colocalization was observed between PV and CR interneurons. Approximately 5.0%, 2.6%, and 4.5% of PV cells and 7.9%, 1.8%, and 2.4% of CR cells colocalized with one another in V1, LIP, and PFC, respectively (Fig. 14A). Overall, colocalization levels remained at an approximate proportion of 10% or less and were therefore determined to be negligible in the current study's assessment of total interneuron densities across cortical areas.
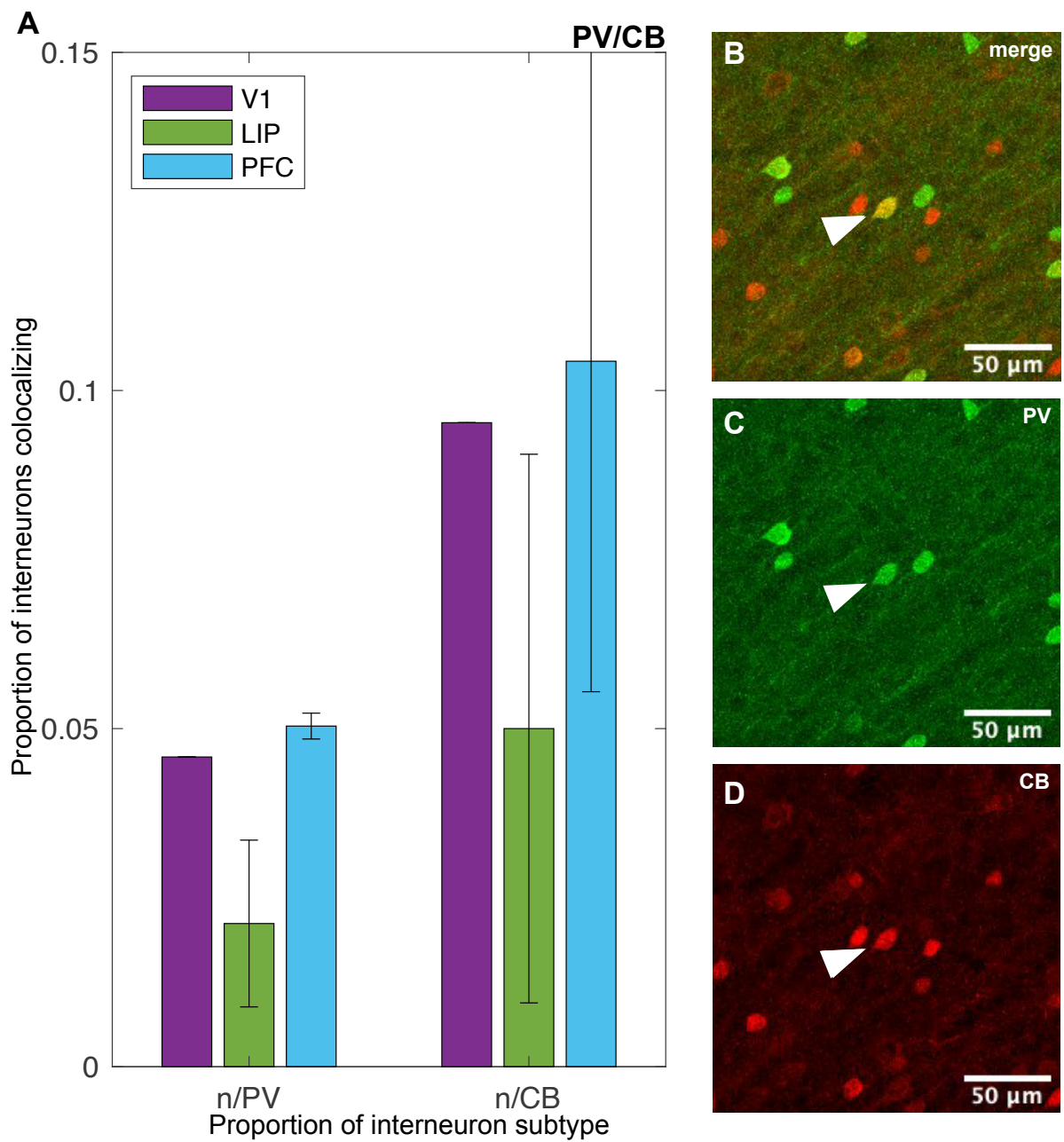
Figure 13. Colocalization of PV/CB markers. Proportions of both PV and CB cells immunoreactive with one another across cortical areas (**A**). Sample images of neurons immunoreactive for PV and CB in cortical area V1 (**B-D**, solid arrowhead). All values shown as mean ± standard deviation.
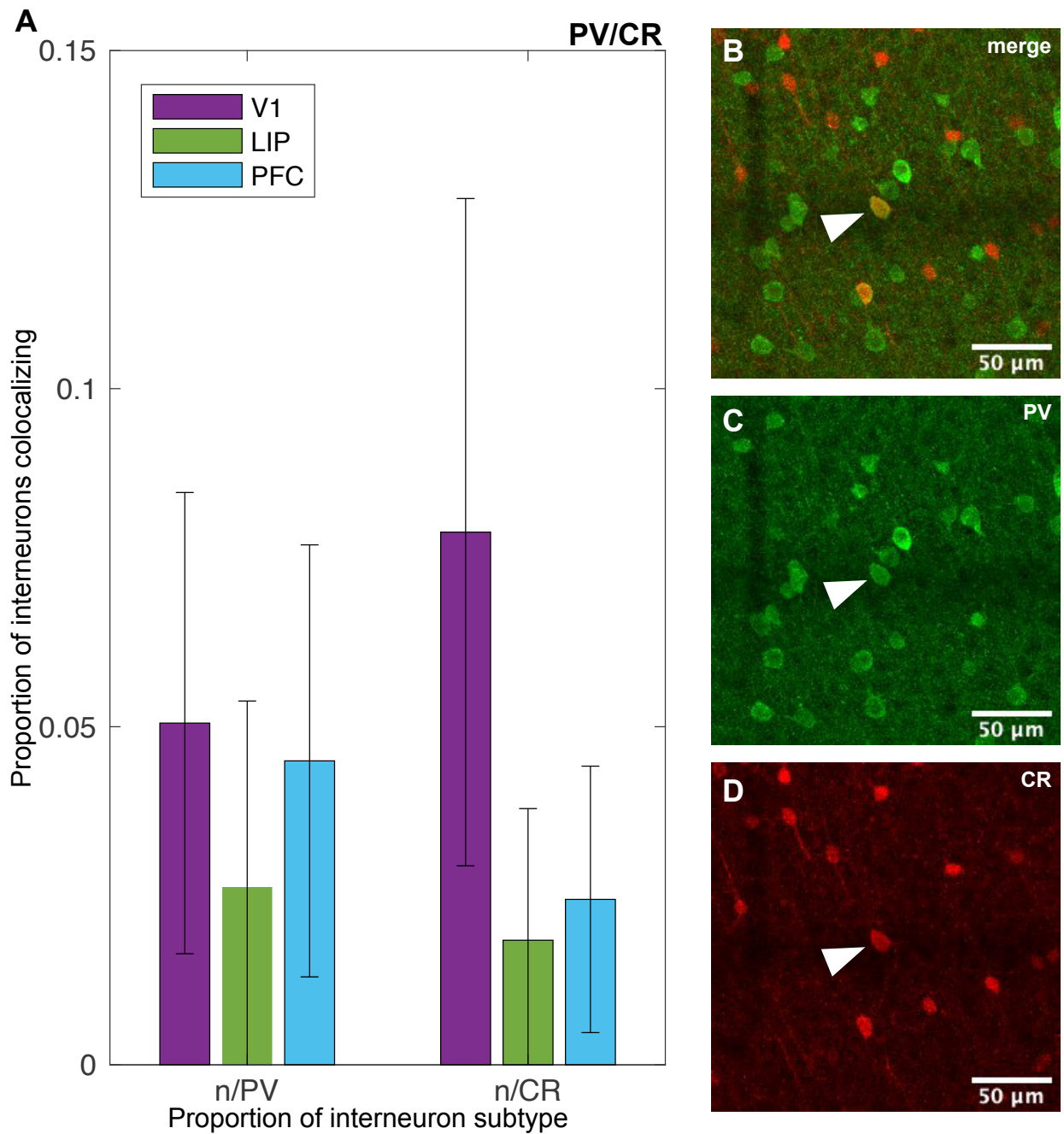
Figure 14. Colocalization of PV/CR markers. Proportions of both PV and CR cells immunoreactive with one another across cortical areas (**A**). Sample images of neurons immunoreactive for PV and CR in cortical area V1 (**B-D**, solid arrowhead). All values shown as mean ± standard deviation.
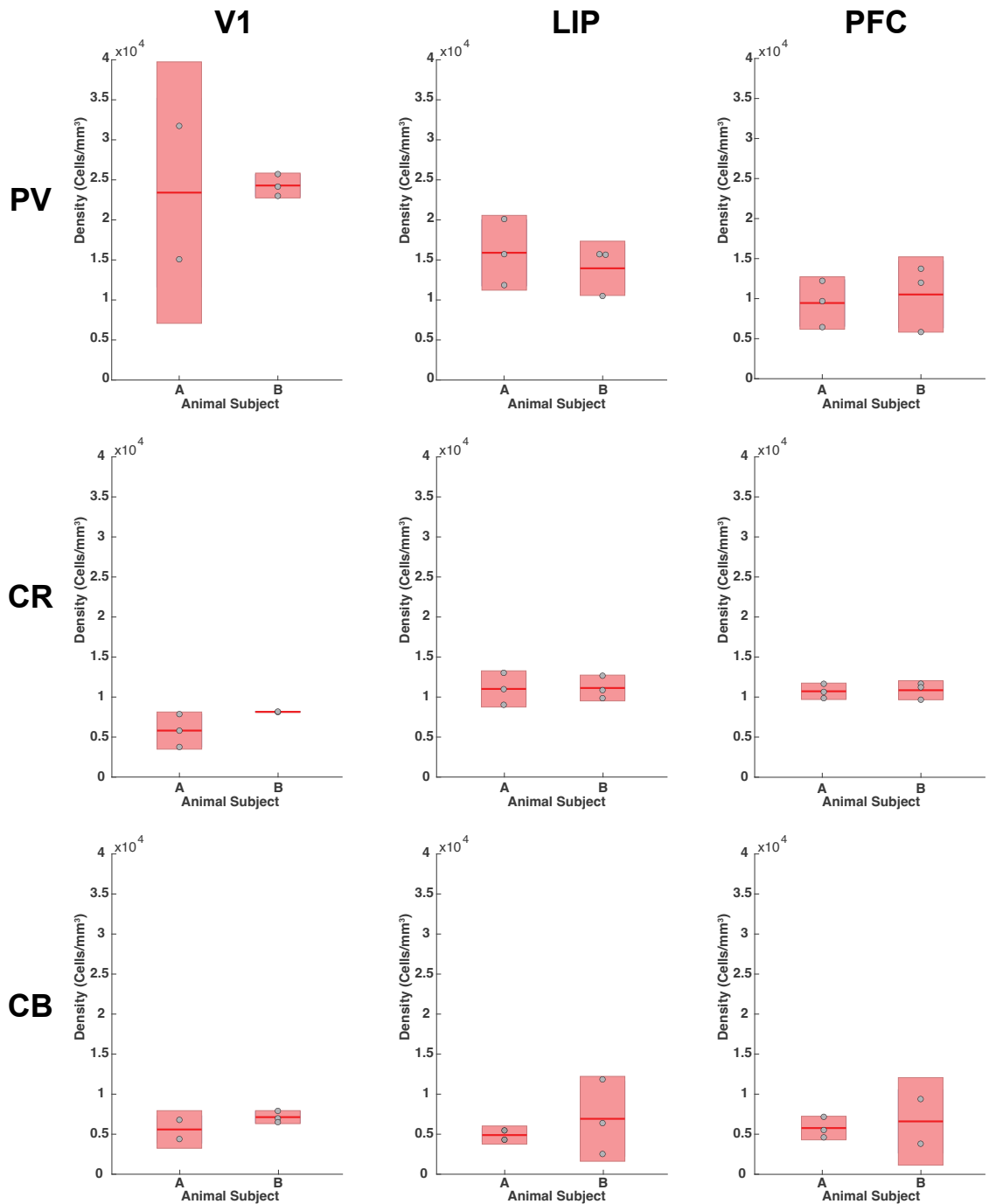
Figure 15. Box plot summary of individual IN cell densities measured from each tissue sample and animal subject within each cortical area. Grey dots represent individual data points. The solid red line represents the median. The bottom and top edges of the boxes represent the 25th and 75th percentiles, respectively.

4 - Discussion

We quantified interneuron abundance across V1, LIP, and PFC and observed no difference in the abundance of CB across cortical areas in terms of their proportions with respect to both total neurons and total interneurons. We did, however, identify differences in relative densities of PV and CR across sensory and association areas. The relative density of PV was significantly lower in PFC compared with V1, while the relative density of CR was significantly greater in LIP and PFC compared with V1. Furthermore, the trends observed in the relative densities of PV and CR across sensory and association areas agree with those observed in a past study exploring the proportions of PV, CB, and CR interneurons across MT, MST, and LPFC in cortical layers II/III of rhesus macaques by Torres-Gomez et al. (2020).

Our results are set apart from those of previous studies exploring interneuron abundance in marmosets due to our approach to quantification of interneuron density by taking into consideration all cortical layers in order to assess laminar distribution, while existing studies quantify interneurons in only a subset of cortical layers (Torres-Gomez et al., 2020). Furthermore, our methodological approach to quantifying interneurons sets us apart from past studies. Antibody penetration during immunostaining is not uniform throughout the entire tissue depth and varies between individual antibodies and tissues (Kim et al., 2015; Fiorelli et al., 2020) and, therefore, may result in misrepresentation of cell quantities when used in stereological methods. Rather than using a constant counting depth across all tissues and histological markers, the current study has implemented a dynamic counting depth that accounts for antibody penetration and minimizes the risk of undercounting cells due to the limits of antibody penetration. In addition, we explore

interneuron abundance in three cortical areas of a visual information processing pathway that spans sensory and association areas, which is yet another characteristic that is absent in past studies assessing laminar distribution and abundance of interneurons in marmosets.

4.1 Overview of cross-area findings in the current study compared with Torres-Gomez et al.

The current study has analyzed the relative densities of PV, CR, and CB interneurons across V1, LIP, and PFC in marmosets while the previous study by Torres-Gomez et al. (2020) explored PV, CR, and CB interneuron densities across cortical areas MT, MST, and LPFC in rhesus macaques. In essence, both studies assess the relative densities of inhibitory interneurons across cortical areas of visual information processing pathways in primates.

4.1.1 General changes in relative densities of interneurons across sensory and association areas

The current study uncovers a significant decrease in the relative density of PV from sensory to association areas, which is in agreement with Torres-Gomez et al.'s observations of a significant decrease in the relative proportion of PV from areas MT to LPFC and from MST to LPFC. These findings are in alignment with the cortical organization principle described by Kim et al. (2017) in rodents stating that sensory areas are dominating by output-modulating PV interneurons.

In addition, the current study observed a significant increase in the relative densities of CR from V1 to LIP and from V1 to PFC, indicating an increasing gradient from sensory to association areas. This finding also agrees with Torres-Gomez et al.'s finding of a

significant increase in the relative proportions of CR from MT to LPFC and from MST to LPFC.

Both studies showed an absence of significant changes in the relative densities/proportions of CB interneurons across cortical areas. In both studies, however, a decrease in CB proportion was expected from sensory areas to LPFC due to its inhibitory nature. However, it could also be argued that an increase in the proportion of CB is to be expected from sensory areas to LPFC due to its input-modulating nature and therefore its potential role in facilitating the maintenance of persistent activity through signal gating and filtration of surrounding distractions. Such functions are necessary for the onset and maintenance of persistent activity in frontal areas responsible for complex cognitive abilities (Wang et al, 2006; Kim et al., 2017). It is possible that the lack of change in CB arises from its seemingly contradicting effects on persistent activity and that it maintains a stable proportion from sensory areas to LPFC to balance its inhibitory effect with its distraction-preventing effects. In addition, it is possible that there is still a change in the extent of the influence that CB cells have across sensory and association areas that arises from the change in proportion of other INs rather than changes in proportions of CB cells themselves. CB cells are the target of CR cells, therefore, the increase that has been observed in CR proportion in LPFC may be sufficient to reduce inhibition by CB and facilitate persistent activity.

4.1.2 *Degree of cross-area changes in current study in comparison to Torres-Gomez et al.*

While both studies showed a similar gradient in the relative proportions of PV and CR, and a lack thereof in CB, across cortical areas, the degree of these changes was more

pronounced across V1, LIP, and PFC in marmosets in our study in comparison to Torres-Gomez et al.'s results across MT, MST and PFC in macaque monkeys. For instance, the proportion of PV cells that comprises the interneuron population decreases by 27.19% from V1 to PFC in the current study and decreases by approximately 5.63% from MT to PFC in Torres-Gomez et al.'s study. In addition, the proportion of CR that comprises the interneuron population increases by 22% from V1 to PFC in the current study while the increase in CR from MT to PFC in Torres-Gomez et al.'s study is reported to be by 6.47% (Table 3).

Such findings of more exaggerated cross-area changes in interneuron proportions in the current study is supported by the greater hierarchical gap between V1 and PFC in the current study compared with the hierarchical gap between MT/MST and LPFC in Torres-Gomez et al.'s study. Area V1 is the earliest visual sensory cortical area and therefore the most highly specialized cortical area. Given that V1 and PFC are on opposite extremes of the cortical hierarchy and have the greatest difference in total neuron density (Atapour et al., 2019), it is evident that the greatest cytoarchitectural jump occurs between V1 and PFC. This cytoarchitectural jump between the areas is likely due to V1's highly specialized nature relative to any other cortical area (Balaram and Kaas, 2014). Therefore, cytoarchitectural changes between PFC and other non-V1 cortical areas, such as MT/MST or LIP, are expected to be much less pronounced regardless of the interneuron subtype in question. As a result, the largest change in the proportion of a given interneuron subtype was expected to occur between V1 and PFC when assessing the findings of the current study and comparing them to those of Torres-Gomez et al., and the findings of both studies are in alignment with such expectations.

4.1.3 Discrepancies in abundance of interneurons between the current study and Torres-Gomez et al.

While both studies describe similar findings with respect to relative changes and interneuron abundances across cortical areas, there are discrepancies between the current study and the past study with respect to the absolute proportions of individual interneurons. Torres-Gomez et al. have underestimated the abundance of PV with respect to its proportion of total interneurons while they have overestimated the abundance of CB and CR with respect to their proportions of total interneurons due to their observations being limited to cortical layers II/III only.

This discrepancy becomes evident when we focus on the common factor between both studies with respect to the cortical area that were explored, the PFC. The current study reports that PV interneurons makeup approximately 37.16% of PFC's interneuron population while Torres-Gomez et al. reported that PV interneurons make up approximately 24.37% of total interneurons (Table 3). It is likely that Torres-Gomez et al. have underestimated PV's abundance because PV interneurons are most abundant in cortical layers IV/V, and by excluding these layers from their observations, Torres-Gomez et al. have overlooked the majority of the PV interneuron population during their cross-area analysis (Van Brederode et al., 1990; DeFelipe et al., 1999; Goodchild and Martin, 1998; Hof et al., 1998; Bourne et al., 2007).

On the contrary, it is likely that CB and CR proportions have been overestimated by Torres-Gomez et al. due to the same limitation in their study. The current study has observed that CB and CR make up approximately 22.69% and 40.14%, respectively, of the interneuron population in PFC. Torres-Gomez et al., on the other hand, have reported that CB and CR make up approximately 26.84% and 48.79%, respectively, of the interneuron

population in PFC. Both CB and CR interneurons are most abundant in superficial cortical layers, such as layers II/III, therefore, Torres-Gomez et al. have likely overestimated the abundance of CB and CR interneurons by limiting the counting window to layers II/III (Hof et al., 1998; Goodchild and Martin, 1998; Hof et al., 1998, Bourne et al., 2007).

There is a possibility that these discrepancies arise from the difference in species; there is an evolutionary expansion of the gPFC in primates and humans have been found to have the greatest expansion compared with other primates (Donahue et al., 2018; Preuss and Wise, 2022). Furthermore, cortical layers II/III were reported to be thicker in humans (Galakhova et al., 2022). Given the closer proximity of macaques to humans than marmosets to humans, it is possible that macaques have thicker cortical layers II/III compared with marmosets, which may account for the higher CR and CB proportions reported by Torres-Gomez et al. in macaques compared with the proportions reported in the current study in marmosets.

4.2 Cross-area comparisons of inhibitory interneurons and their functional relevance

Considering that both the current study and the past study by Torres-Gomez et al. reported similar findings with respect to general trends in inhibitory interneurons across sensory and association areas of primates, it is likely that such spatial distributions have a functional relevance.

4.2.1 Greater CR abundance in LIP and PFC compared with V1

The finding that CR density is significantly greater in LIP and PFC is consistent with the findings of past primate studies. For instance, Ma et al. (2013) reports a significantly higher proportion of CR interneurons in parietal and frontal areas compared

with other cortical areas in primates. In addition, Yan et al. (1995) reported that 20% of GABAergic neurons are CR-immunoreactive in the primary visual area of macaque monkeys, while Dzâja et al. (2014) calculated CR abundance in frontal lobes of monkeys from the data gathered in several past studies and reported that 28.6-44.8% of GABAergic neurons in the frontal lobe were CR-immunoreactive. Rodents, on the other hand, did not demonstrate an increase in CR abundance in their frontal lobe compared with V1 (Dzâja et al., 2014). Considering the similarity in frontal lobe organization between marmosets and macaques (Burman et al., 2006), along with the greater evolutionary proximity of marmosets to macaques as opposed to rodents, we expect the abundance and distribution of CR across cortical areas in marmosets to display similar patterns to those observed in macaques rather than those observed in rodents.

The observation of increased CR densities in LIP and PFC supports the idea that there is a difference in the interneuron composition, with respect to relative proportions of inhibitory interneurons, of sensory areas compared with association areas. Furthermore, the functional relevance of an increased CR abundance in association areas may be linked to CR's disinhibitory effect. The disinhibitory nature of CR contributes to its role in promoting persistent activity of pyramidal cells within neuronal networks in a localized manner. This continuous pattern of microcircuit activation has been shown to correlate with the presence of higher order cognitive functions, specifically in dorsolateral PFC (Finn et al., 2019; Wang & Yang, 2018; Wang et al., 2004). For instance, a visual delayed-response task in macaque monkeys uncovered activity persisting into the delay period in LPFC neurons but not in MT neurons (Mendoza-Halliday et al., 2014).

In addition to increased CR influence, increased CR density may also be an indicator of LIP and PFC's increased ability to fine-tune microcircuit activation compared

with V1. The presence of an increased CR density and lower total neuron densities in LIP and PFC compared with V1 (Atapour et al., 2019) indicated an increased CR interneuron to pyramidal cell ratio. This increased ratio suggests that individual CR interneurons in LIP and PFC synapse with a smaller, more distinct number of target cells when compared with V1, providing potential for fine-tuning of signals.

Upon observing a significant difference in CR abundance across cortical areas, a closer look was taken at its laminar distribution profile within each area. This examination revealed the same laminar distribution pattern across all three cortical areas; a significantly greater proportion of total CR localized to layer II than in any other cortical layer. This finding is consistent with past primate studies reporting greater proportions of CR in upper cortical layers and that the extent of this localization of CR to the upper layers is more prominent in association areas (Džaja et al., 2014). Given that CR cells originate in the central ganglionic eminence (CGE) and thus migrate into the cortex (Gelman et al., 2012; Lodato et al., 2011), our findings suggest that localization of CR predominantly to layer II is not a random occurrence, rather that it has a functional relevance; in the absence of a functional relevance, it is likely that the cells would migrate at random throughout the cortex without localizing to a specific cortical layer across different cortical regions. Furthermore, it is known that an evolutionary expansion of cortical layers II and III occur in primates, including marmosets (Preuss and Wise, 2022; Elston et al., 2005). The expansion of layers II and III, the layers in which CR cell somata are predominantly located, in conjunction with our findings of greater CR density in LIP and PFC compared with V1 provide further support for the presence of a hierarchical gradient in interneuron density across sensory and association areas in marmosets.

4.2.2 *Greater PV abundance in V1 compared with PFC*

We observed a significantly greater relative density of PV cells in V1 compared with LIP and PFC which is supported by the role that PV interneurons play in mediating excitatory activity. PV cells are known to play a significant role in mediating the synchronous oscillatory activity that facilitates stimulus selectivity in V1 and transmission of information to higher brain regions (Felleman and Van Essen, 1991; Onorato, et al., 2020). In addition, PV cells' role in primarily targeting pyramidal cells at a peri-somatic level to produce wide-spread inhibition suggests its role as an input-modulating interneuron and therefore its potential function in suppressing the high volume of inputs to V1 to allow for orientation selectivity. This role of PV cells has been observed in V1 of mice; optogenetic activation of PV cells in mouse V1 was shown to improve orientation discrimination and overall neuronal feature selectivity. Moreover, optogenetic activation of other inhibitory interneuron subtypes produced no significant difference in orientation discrimination and feature selectivity, suggesting that such functions may be specific to PV interneurons (Lee et al., 2012). In addition, Naka and Adesnik (2016) have described the reliable yet precisely timed and fast-spiking nature of PV's inhibitory signals in sensory areas of marmosets, and how such features contribute to its role in precise temporal coding of sensory stimuli. Such precision and temporal-specificity of PV's firing patterns further support PV's crucial role in allowing for orientation selectivity in V1 and therefore its significantly greater relative density in this cortical area. Such functional components of PV interneurons agree with Kim et al. (2017), a study in which Kim et al. have described a principle that consists of an increased abundance of output-modulating PV cells in sensory areas of rodents.

Given that V1 is present in both primates and rodents and that its orientation selectivity function is preserved in both types of species (Kaas and Collins, 2001; Niell & Stryker, 2008; Liska et al., 2022), it is likely that the mechanisms underlying such selectivity in sensory areas of rodents are conserved between rodents and primates. In other words, the involvement of PV interneurons in stimulus selectivity and PV's gradient across cortical areas of primates are likely to follow similar patterns to those described by Lee et al. (2012) and Kim et al. (2017) in rodents.

The laminar distribution of PV further supports its increased abundance in V1 and its functional relevance to V1. We observed significantly greater abundance of PV interneurons in layer IV compared with any other cortical layer, which is supported by the characteristic laminar distribution of PV interneurons that has been described by previous studies (Van Brederode et al., 1990; DeFelipe et al., 1999; Goodchild and Martin, 1998; Hof et al., 1998; Bourne et al., 2007). Furthermore, cortical layer IV is known to be cortical layer that receives the greatest number of thalamic inputs and therefore the primary site at which sensory inputs enter (Zhuang et al., 2013). Therefore, the localization of PV cells primarily to cortical layer IV facilitates the ability of this interneuron subtype to target pyramidal cells at a peri-somatic level and to produce wide-spread inhibition at the primary site of sensory input entry into V1. Such wide-spread inhibition at the site of input entry likely contributes to the mechanism underlying stimulus selectivity in V1 by allowing for the filtration of the high number of inputs.

4.2.3   No changes in CB abundance across cortical areas

The principle of cortical organization described by Kim et al. (2017) supports an increase in input-modulating SST-containing interneurons from early sensory areas to

association areas. Given that SST interneurons in mice are believed to be equivalent to CB interneurons in primates (Kubota et al., 1994; Kawaguchi and Kubota, 1997), we expected similar observations with respect to CB cells in the current study.

We did not, however, observe any significant changes in the relative density of CB cells across cortical areas, nor did Torres-Gomez et al. in their study (2020). This discrepancy may be due to the fact that this principle originated in rodents while the current studies examine primate models. Furthermore, it is possible that CB interneurons in association areas of primates have greater influence relative to early sensory areas without necessarily reflecting this increased influence in their cell abundance. While we did not observe any differences in the relative density of CB across sensory and association areas on the level of protein expression, our findings do not eliminate the possibility that CB interneurons differ on a single-cell level between cortical areas. Morphological differences between cortical areas for a given cell type may determine the influence that the cell has on its surroundings and may provide another means by which a hierarchical gradient across sensory and association areas may be characterized. For instance, CB interneurons in association areas of primates may differ morphologically from those in their early sensory areas such that they develop greater dendritic arborization and therefore synapse with a greater number of surrounding cells. If CB interneurons are found to demonstrate such morphological changes in association areas, this would suggest that CB interneurons have a greater influence in association areas compared with sensory areas in a manner that supports the model described by Kim et al. (2017) while accounting for the findings of Torres-Gomez et al. (2020) and the current study with respect to the lack of change in CB abundance across cortical areas.

4.2.4   Colocalization of PV/CB and PV/CR

Colocalization of PV/CB and PV/CR were both found to account for approximately 10% of detected INs or less and, therefore, was deemed to be negligible in the context of the cross-area results that were observed. Low levels of colocalization have been observed in past primate studies (Hendry et al., 1989; Van Brederode et al., 1990; Meskenaite et al., 1997; Leuba et al., 1998) but it remains unclear how colocalization levels compare across cortical areas, specifically in the context of marmosets. Detection of colocalization may also potentially result from signal leak between channels during the imaging stage given the excitation wavelengths of the conjugated secondary antibodies used for PV, CB, and CR. The excitation wavelength of the fluorophore used in PV detection was 546 nm while that of the fluorophore used in CB and CR detection was 657 nm. Imaging parameters were optimized to minimize signal leak between adjacent channels as much as possible but this may still account for some of the colocalization that was observed.

Large error bars were generated during statistical analysis of colocalization measures, and this is likely due to the low observation of colocalizing cells; colocalization was rare and often absent from most tissues, therefore, detection of colocalization acted as an 'outlier' in the data. The large error bars are likely a result of the rarity of colocalization detection combined with the sensitivity of standard deviation to outlier values.

4.3 Future Directions

Future studies may consider assessing morphological and physiological properties of interneuron subtypes across cortical areas to determine whether a hierarchical gradient is present across cortical areas at the single-cell level. Since axon length and density provide an estimate of the functional impact of a given neuron (Rubio-Teves et al., 2021), future studies may consider comparing axon and dendrite morphologies of the interneuron

subtypes across sensory and association areas to uncover other potential cross-area hierarchies. While the current study uncovered hierarchies with respect to cell abundance for PV and CR interneurons, other cross-area changes may also exist, particularly for CB interneurons, which did not display any cross-area changes in the current study. For instance, it is possible that CB cells in PFC are more divergent than CB cells in V1, such that a single CB cell in PFC would have a greater influence on its surrounding neurons than a less divergent CB cell in V1, in order to facilitate CB's role in preventing distracting inputs from interfering with persistent activity. Such findings may contribute to improving our understanding of the mechanisms underlying the role that each interneuron plays in supporting the functions of different cortical areas.

In addition, recent findings have demonstrated that the granular prefrontal cortex expands in accordance with species' cognitive complexity, suggesting that a larger-scale hierarchy may exist not only across brain regions, but across species as well. While both New World marmosets and Old World macaques demonstrate evolutionary expansion of granular PFC, the extent of this expansion is greater in macaques compared with marmosets (Elston et al., 2005). Future studies should assess cross-species hierarchies with respect to interneuron gradients across cortical areas by analyzing interneuron distribution and abundance in both Old World macaques and New World mamorsets and conducting a cross-species comparison. It is expected that the hierarchical gradient observed in the current study will be more pronounced in Old World Macaques due to increased cognitive complexity and the greater extent of granular PFC expansion in these species (Elston et al., 2005; Preuss & Wise, 2022).

4.4 Conclusion

The findings of the current study show that relative interneuron subtype proportions differ across sensory and association areas in accordance with area complexity in the common marmoset. The characteristic laminar distributions for each interneuron subtype, however, remain consistent across cortical areas. These findings improve our understanding of how microcircuit organization and the spatial distribution of inhibitory interneurons contribute to the mechanism underlying higher-order cognitive functions associated with the dorsolateral PFC.

References

Atapour, N., Majka, P., Wolkowicz, I. H., Malamanova, D., Worthy, K. H., & Rosa, M. G. P. (2019). Neuronal Distribution Across the Cerebral Cortex of the Marmoset Monkey (Callithrix jacchus). *Cerebral Cortex (New York, N.Y.: 1991)*, *29*(9), 3836–3863. https://doi.org/10.1093/cercor/bhy263

Balaram, P., & Kaas, J. H. (2014). Towards a unified scheme of cortical lamination for primary visual cortex across primates: Insights from NeuN and VGLUT2 immunoreactivity. *Frontiers in Neuroanatomy*, *8*, 81. https://doi.org/10.3389/fnana.2014.00081

Baslow, M. H. (2011). The Vertebrate Brain, Evidence of Its Modular Organization and Operating System: Insights into the Brain's Basic Units of Structure, Function, and Operation and How They Influence Neuronal Signaling and Behavior. *Frontiers in Behavioral Neuroscience*, *5*, 5. https://doi.org/10.3389/fnbeh.2011.00005

Beasley, C. L., & Reynolds, G. P. (1997). Parvalbumin-immunoreactive neurons are reduced in the prefrontal cortex of schizophrenics. *Schizophrenia Research*, *24*(3), 349–355. https://doi.org/10.1016/s0920-9964(96)00122-3

Bianchi, S., Stimpson, C. D., Bauernfeind, A. L., Schapiro, S. J., Baze, W. B., McArthur, M. J., Bronson, E., Hopkins, W. D., Semendeferi, K., Jacobs, B., Hof, P. R., & Sherwood, C. C. (2013). Dendritic Morphology of Pyramidal Neurons in the Chimpanzee Neocortex: Regional Specializations and Comparison to Humans. *Cerebral Cortex (New York, NY)*, *23*(10), 2429–2436. https://doi.org/10.1093/cercor/bhs239

Bisley, J. W., & Goldberg, M. E. (2003). Neuronal activity in the lateral intraparietal area and spatial attention. *Science (New York, N.Y.)*, *299*(5603), 81–86. https://doi.org/10.1126/science.1077395

Bisley, J. W., Mirpour, K., Arcizet, F., & Ong, W. S. (2011). The Role of the Lateral Intraparietal Area in Orienting Attention and its Implications for Visual Search. *The European Journal of Neuroscience*, *33*(11), 1982–1990. https://doi.org/10.1111/j.1460-9568.2011.07700.x

Bourne, J. A., Warner, C. E., Upton, D. J., & Rosa, M. G. P. (2007). Chemoarchitecture of the middle temporal visual area in the marmoset monkey (Callithrix jacchus): Laminar distribution of calcium-binding proteins (calbindin, parvalbumin) and nonphosphorylated neurofilament. *The Journal of Comparative Neurology*, *500*(5), 832–849. https://doi.org/10.1002/cne.21190

Burman, K. J., Palmer, S. M., Gamberini, M., & Rosa, M. G. P. (2006). Cytoarchitectonic subdivisions of the dorsolateral frontal cortex of the marmoset monkey (Callithrix jacchus), and their projections to dorsal visual areas. *The Journal of Comparative Neurology*, *495*(2), 149–172. https://doi.org/10.1002/cne.20837

Bushnell, M. C., Goldberg, M. E., & Robinson, D. L. (1981). Behavioral enhancement of visual responses in monkey cerebral cortex. I. Modulation in posterior parietal cortex related to selective visual attention. *Journal of Neurophysiology*, *46*(4), 755–772. https://doi.org/10.1152/jn.1981.46.4.755

Cela-Conde, C. J., Lombardo, R. G., Avise, J. C., & Ayala, F. J. (Eds.). (2014). *In the Light of Evolution: Volume VII: The Human Mental Machinery* (Vol. 7). National Academies Press (US). http://www.ncbi.nlm.nih.gov/books/NBK231629/

Condé, F., Lund, J. S., Jacobowitz, D. M., Baimbridge, K. G., & Lewis, D. A. (1994). Local circuit neurons immunoreactive for calretinin, calbindin D-28k or parvalbumin in monkey prefrontal cortex: Distribution and morphology. *The Journal of Comparative Neurology*, *341*(1), 95–116. https://doi.org/10.1002/cne.903410109

Constantinidis, C., Funahashi, S., Lee, D., Murray, J. D., Qi, X.-L., Wang, M., & Arnsten, A. F. T. (2018). Persistent Spiking Activity Underlies Working Memory. *The Journal of Neuroscience: The Official Journal of the Society for Neuroscience*, *38*(32), 7020–7028. https://doi.org/10.1523/JNEUROSCI.2486-17.2018

Defelipe, J., González-Albo, M. C., Del Río, M. R., & Elston, G. N. (1999). Distribution and patterns of connectivity of interneurons containing calbindin, calretinin, and parvalbumin in visual areas of the occipital and temporal lobes of the macaque monkey. *The Journal of Comparative Neurology*, *412*(3), 515–526. https://doi.org/10.1002/(sici)1096-9861(19990927)412:3<515::aid-cne10>3.0.co;2-1

D'Esposito, M., Detre, J. A., Alsop, D. C., Shin, R. K., Atlas, S., & Grossman, M. (1995). The neural basis of the central executive system of working memory. *Nature*, *378*(6554), 279–281. https://doi.org/10.1038/378279a0

Donahue, C. J., Glasser, M. F., Preuss, T. M., Rilling, J. K., & Van Essen, D. C. (2018). Quantitative assessment of prefrontal cortex in humans relative to nonhuman primates. *Proceedings of the National Academy of Sciences of the United States of America*, *115*(22), E5183–E5192. https://doi.org/10.1073/pnas.1721653115

Džaja, D., Hladnik, A., Bičanić, I., Baković, M., & Petanjek, Z. (2014). Neocortical calretinin neurons in primates: Increase in proportion and microcircuitry structure. *Frontiers in Neuroanatomy*, *8*, 103. https://doi.org/10.3389/fnana.2014.00103

Elston, G. N., Benavides-Piccione, R., Elston, A., Zietsch, B., Defelipe, J., Manger, P., Casagrande, V., & Kaas, J. H. (2006). Specializations of the granular prefrontal cortex of primates: Implications for cognitive processing. *The Anatomical Record. Part A, Discoveries in Molecular, Cellular, and Evolutionary Biology*, *288*(1), 26–35. https://doi.org/10.1002/ar.a.20278

Feizpour, A., Majka, P., Chaplin, T. A., Rowley, D., Yu, H.-H., Zavitz, E., Price, N. S. C., Rosa, M. G. P., & Hagan, M. A. (2021). Visual responses in the dorsolateral frontal cortex of marmoset monkeys. *Journal of Neurophysiology*, *125*(1), 296–304. https://doi.org/10.1152/jn.00581.2020

Felleman, D. J., & Van Essen, D. C. (1991). Distributed hierarchical processing in the primate cerebral cortex. *Cerebral Cortex (New York, N.Y.: 1991)*, *1*(1), 1–47. https://doi.org/10.1093/cercor/1.1.1-a

Finn, E. S., Huber, L., Jangraw, D. C., Molfese, P. J., & Bandettini, P. A. (2019). Layer-dependent activity in human prefrontal cortex during working memory. *Nature Neuroscience*, *22*(10), 1687–1695. https://doi.org/10.1038/s41593-019-0487-z

Fiorelli, R., Sidhu, G., Cebrián-Silla, A., Melendez, E. L., Mehta, S., Garcia-Verdugo, J., & Sanai, N. (2020). *Enhanced tissue penetration of antibodies through pressurized immunohistochemistr*. https://doi.org/10.1101/2020.09.25.311936

Galakhova, A. A., Hunt, S., Wilbers, R., Heyer, D. B., de Kock, C. P. J., Mansvelder, H. D., & Goriounova, N. A. (2022). Evolution of cortical neurons supporting human cognition. *Trends in Cognitive Sciences*, *26*(11), 909–922. https://doi.org/10.1016/j.tics.2022.08.012

Gelman, D. M., Marín, O., & Rubenstein, J. L. R. (2012). The Generation of Cortical Interneurons. In J. L. Noebels, M. Avoli, M. A. Rogawski, R. W. Olsen, & A. V. Delgado-Escueta (Eds.), *Jasper's Basic Mechanisms of the Epilepsies* (4th ed.). National Center for Biotechnology Information (US). http://www.ncbi.nlm.nih.gov/books/NBK98190/

Goldman-Rakic, P. S. (1995). Cellular basis of working memory. *Neuron*, *14*(3), 477–485. https://doi.org/10.1016/0896-6273(95)90304-6

Goodale, M. A. (1993). Visual pathways supporting perception and action in the primate cerebral cortex. *Current Opinion in Neurobiology*, *3*(4), 578–585. https://doi.org/10.1016/0959-4388(93)90059-8

Goodchild, A. K., & Martin, P. R. (1998). The distribution of calcium-binding proteins in the lateral geniculate nucleus and visual cortex of a New World monkey, the marmoset, Callithrix jacchus. *Visual Neuroscience*, *15*(4), 625–642. https://doi.org/10.1017/s0952523898154044

Hendry, S. H., Jones, E. G., Emson, P. C., Lawson, D. E., Heizmann, C. W., & Streit, P. (1989). Two classes of cortical GABA neurons defined by differential calcium binding protein immunoreactivities. *Experimental Brain Research*, *76*(2), 467–472. https://doi.org/10.1007/BF00247904

Hof, P. R., Glezer, I. I., Condé, F., Flagg, R. A., Rubin, M. B., Nimchinsky, E. A., & Vogt Weisenhorn, D. M. (1999). Cellular distribution of the calcium-binding proteins parvalbumin, calbindin, and calretinin in the neocortex of mammals: Phylogenetic and developmental patterns. *Journal of Chemical Neuroanatomy*, *16*(2), 77–116. https://doi.org/10.1016/s0891-0618(98)00065-9

Kaas, J. H., & Collins, C. E. (2001). The organization of sensory cortex. *Current Opinion in Neurobiology*, *11*(4), 498–504. https://doi.org/10.1016/s0959-4388(00)00240-3

Kawaguchi, Y., & Kubota, Y. (1997). GABAergic cell subtypes and their synaptic connections in rat frontal cortex. *Cerebral Cortex (New York, N.Y.: 1991)*, *7*(6), 476–486. https://doi.org/10.1093/cercor/7.6.476

Kell, A. J. E., Bokor, S. L., Jeon, Y.-N., Toosi, T., & Issa, E. B. (2023). Marmoset core visual object recognition behavior is comparable to that of macaques and humans. *iScience*, *26*(1), 105788. https://doi.org/10.1016/j.isci.2022.105788

Kim, S.-Y., Cho, J. H., Murray, E., Bakh, N., Choi, H., Ohn, K., Ruelas, L., Hubbert, A., McCue, M., Vassallo, S. L., Keller, P. J., & Chung, K. (2015). Stochastic electrotransport selectively enhances the transport of highly electromobile molecules. *Proceedings of the National Academy of Sciences of the United States of America*, *112*(46), E6274-6283. https://doi.org/10.1073/pnas.1510133112

Kim, Y., Yang, G. R., Pradhan, K., Venkataraju, K. U., Bota, M., García Del Molino, L. C., Fitzgerald, G., Ram, K., He, M., Levine, J. M., Mitra, P., Huang, Z. J., Wang, X.-J., & Osten, P. (2017). Brain-wide Maps Reveal Stereotyped Cell-Type-Based Cortical Architecture and Subcortical Sexual Dimorphism. *Cell*, *171*(2), 456-469.e22. https://doi.org/10.1016/j.cell.2017.09.020

Kimberg, D. Y., D'Esposito, M., & Farah, M. J. (1997). Cognitive Functions in the Prefrontal Cortex: Working Memory and Executive Control. *Current Directions in Psychological Science*, *6*(6), 185–192.

Koechlin, E., Basso, G., Pietrini, P., Panzer, S., & Grafman, J. (1999). The role of the anterior prefrontal cortex in human cognition. *Nature*, *399*(6732), 148–151. https://doi.org/10.1038/20178

Kooijmans, R. N., Sierhuis, W., Self, M. W., & Roelfsema, P. R. (2020). A Quantitative Comparison of Inhibitory Interneuron Size and Distribution between Mouse and Macaque V1, Using Calcium-Binding Proteins. *Cerebral Cortex Communications*, *1*(1), tgaa068. https://doi.org/10.1093/texcom/tgaa068

Kubota, Y., Hattori, R., & Yui, Y. (1994). Three distinct subpopulations of GABAergic neurons in rat frontal agranular cortex. *Brain Research*, *649*(1–2), 159–173. https://doi.org/10.1016/0006-8993(94)91060-x

Lee, S.-H., Kwan, A. C., Zhang, S., Phoumthipphavong, V., Flannery, J. G., Masmanidis, S. C., Taniguchi, H., Huang, Z. J., Zhang, F., Boyden, E. S., Deisseroth, K., & Dan, Y. (2012). Activation of specific interneurons improves V1 feature selectivity and visual perception. *Nature*, *488*(7411), 379–383. https://doi.org/10.1038/nature11312

Leuba, G., Kraftsik, R., & Saini, K. (1998). Quantitative distribution of parvalbumin, calretinin, and calbindin D-28k immunoreactive neurons in the visual cortex of normal and Alzheimer cases. *Experimental Neurology*, *152*(2), 278–291. https://doi.org/10.1006/exnr.1998.6838

Liska, J. P., Rowley, D. P., Nguyen, T. T. K., Muthmann, J.-O., Butts, D. A., Yates, J. L., & Huk, A. C. (2023). *Running modulates primate and rodent visual cortex differently* (p. 2022.06.13.495712). bioRxiv. https://doi.org/10.1101/2022.06.13.495712

Lodato, S., Tomassy, G. S., De Leonibus, E., Uzcategui, Y. G., Andolfi, G., Armentano, M., Touzot, A., Gaztelu, J. M., Arlotta, P., Menendez de la Prida, L., & Studer, M. (2011). Loss of COUP-TFI alters the balance between caudal ganglionic eminence- and medial ganglionic eminence-derived cortical interneurons and results in resistance to epilepsy. *The Journal of Neuroscience: The Official Journal of the Society for Neuroscience*, *31*(12), 4650–4662. https://doi.org/10.1523/JNEUROSCI.6580-10.2011

Lui, L. L., & Rosa, M. G. P. (2015). Structure and function of the middle temporal visual area (MT) in the marmoset: Comparisons with the macaque monkey. *Neuroscience Research*, *93*, 62–71. https://doi.org/10.1016/j.neures.2014.09.012

Ma, T., Wang, C., Wang, L., Zhou, X., Tian, M., Zhang, Q., Zhang, Y., Li, J., Liu, Z., Cai, Y., Liu, F., You, Y., Chen, C., Campbell, K., Song, H., Ma, L., Rubenstein, J. L., & Yang, Z. (2013). Subcortical origins of human and monkey neocortical interneurons. *Nature Neuroscience*, *16*(11), 1588–1597. https://doi.org/10.1038/nn.3536

Malhotra, P., Coulthard, E. J., & Husain, M. (2009). Role of right posterior parietal cortex in maintaining attention to spatial locations over time. *Brain: A Journal of Neurology*, *132*(Pt 3), 645–660. https://doi.org/10.1093/brain/awn350

Manoach, D. S., Schlaug, G., Siewert, B., Darby, D. G., Bly, B. M., Benfield, A., Edelman, R. R., & Warach, S. (1997). Prefrontal cortex fMRI signal changes are correlated with working memory load. *Neuroreport*, *8*(2), 545–549. https://doi.org/10.1097/00001756-199701200-00033

Mars, R. B., & Grol, M. J. (2007). Dorsolateral prefrontal cortex, working memory, and prospective coding for action. *The Journal of Neuroscience: The Official Journal of the Society for Neuroscience*, *27*(8), 1801–1802. https://doi.org/10.1523/jneurosci.5344-06.2007

Mashiko, H., Yoshida, A. C., Kikuchi, S. S., Niimi, K., Takahashi, E., Aruga, J., Okano, H., & Shimogori, T. (2012). Comparative anatomy of marmoset and mouse cortex from genomic expression. *The Journal of Neuroscience: The Official Journal of the Society for Neuroscience*, *32*(15), 5039–5053. https://doi.org/10.1523/JNEUROSCI.4788-11.2012

Mendoza-Halliday, D., Torres, S., & Martinez-Trujillo, J. C. (2014). Sharp emergence of feature-selective sustained activity along the dorsal visual pathway. *Nature Neuroscience*, *17*(9), 1255–1262. https://doi.org/10.1038/nn.3785

Meskenaite, V. (1997). Calretinin-immunoreactive local circuit neurons in area 17 of the cynomolgus monkey, Macaca fascicularis. *The Journal of Comparative Neurology*, *379*(1), 113–132.

Miller, C. T., Freiwald, W. A., Leopold, D. A., Mitchell, J. F., Silva, A. C., & Wang, X. (2016). Marmosets: A Neuroscientific Model of Human Social Behavior. *Neuron*, *90*(2), 219–233. https://doi.org/10.1016/j.neuron.2016.03.018

Miyashita, Y. (2022). Operating principles of the cerebral cortex as a six-layered network in primates: Beyond the classic canonical circuit model. *Proceedings of the Japan Academy. Series B, Physical and Biological Sciences*, *98*(3), 93–111. https://doi.org/10.2183/pjab.98.007

Naka, A., & Adesnik, H. (2016). Inhibitory Circuits in Cortical Layer 5. *Frontiers in Neural Circuits*, *10*, 35. https://doi.org/10.3389/fncir.2016.00035

Niell, C. M., & Stryker, M. P. (2008). Highly selective receptive fields in mouse visual cortex. *The Journal of Neuroscience: The Official Journal of the Society for Neuroscience*, *28*(30), 7520–7536. https://doi.org/10.1523/JNEUROSCI.0623-08.2008

Onorato, I., Neuenschwander, S., Hoy, J., Lima, B., Rocha, K.-S., Broggini, A. C., Uran, C., Spyropoulos, G., Klon-Lipok, J., Womelsdorf, T., Fries, P., Niell, C., Singer, W., & Vinck, M. (2020). A Distinct Class of Bursting Neurons with Strong Gamma Synchronization and Stimulus Selectivity in Monkey V1. *Neuron*, *105*(1), 180-197.e5. https://doi.org/10.1016/j.neuron.2019.09.039

Paxinos, G., Petrides, M., Tokuno, H., Watson, C., & Rosa, M. (2012). *The Marmoset Brain in Stereotaxic Coordinates* (1st ed.). Elsevier.

Petilla Interneuron Nomenclature Group, Ascoli, G. A., Alonso-Nanclares, L., Anderson, S. A., Barrionuevo, G., Benavides-Piccione, R., Burkhalter, A., Buzsáki, G., Cauli, B., Defelipe, J., Fairén, A., Feldmeyer, D., Fishell, G., Fregnac, Y., Freund, T. F., Gardner, D., Gardner, E. P., Goldberg, J. H., Helmstaedter, M., … Yuste, R. (2008). Petilla terminology: Nomenclature of features of GABAergic interneurons of the cerebral cortex. *Nature Reviews. Neuroscience*, *9*(7), 557–568. https://doi.org/10.1038/nrn2402

Pollock, E., Everest, M., Brown, A., & Poulter, M. O. (2014). Metalloproteinase inhibition prevents inhibitory synapse reorganization and seizure genesis. *Neurobiology of Disease*, *70*, 21–31. https://doi.org/10.1016/j.nbd.2014.06.003

Preuss, T. M., & Wise, S. P. (2022). Evolution of prefrontal cortex. *Neuropsychopharmacology: Official Publication of the American College of Neuropsychopharmacology*, *47*(1), 3–19. https://doi.org/10.1038/s41386-021-01076-5

Qi, X.-L., Katsuki, F., Meyer, T., Rawley, J. B., Zhou, X., Douglas, K. L., & Constantinidis, C. (2010). Comparison of neural activity related to working memory in primate dorsolateral prefrontal and posterior parietal cortex. *Frontiers in Systems Neuroscience*, *4*, 12. https://doi.org/10.3389/fnsys.2010.00012

Rubio-Teves, M., Díez-Hermano, S., Porrero, C., Sánchez-Jiménez, A., Prensa, L., Clascá, F., García-Amado, M., & Villacorta-Atienza, J. A. (2021). Benchmarking of tools for axon length measurement in individually-labeled projection neurons. *PLoS Computational Biology*, *17*(12), e1009051. https://doi.org/10.1371/journal.pcbi.1009051

Sheth, B. R., & Young, R. (2016). Two Visual Pathways in Primates Based on Sampling of Space: Exploitation and Exploration of Visual Information. *Frontiers in Integrative Neuroscience*, *10*, 37. https://doi.org/10.3389/fnint.2016.00037

Shimogori, T., Abe, A., Go, Y., Hashikawa, T., Kishi, N., Kikuchi, S. S., Kita, Y., Niimi, K., Nishibe, H., Okuno, M., Saga, K., Sakurai, M., Sato, M., Serizawa, T., Suzuki, S., Takahashi, E., Tanaka, M., Tatsumoto, S., Toki, M., … Okano, H. (2018). Digital gene atlas of neonate common marmoset brain. *Neuroscience Research*, *128*, 1–13. https://doi.org/10.1016/j.neures.2017.10.009

Torres-Gomez, S., Blonde, J. D., Mendoza-Halliday, D., Kuebler, E., Everest, M., Wang, X. J., Inoue, W., Poulter, M. O., & Martinez-Trujillo, J. (2020). Changes in the Proportion of Inhibitory Interneuron Types from Sensory to Executive Areas of the Primate Neocortex: Implications for the Origins of Working Memory Representations. *Cerebral Cortex (New York, N.Y.: 1991)*, *30*(8), 4544–4562. https://doi.org/10.1093/cercor/bhaa056

Uncapher, M. R., & Wagner, A. D. (2009). Posterior parietal cortex and episodic encoding: Insights from fMRI subsequent memory effects and dual-attention theory. *Neurobiology of Learning and Memory*, *91*(2), 139–154. https://doi.org/10.1016/j.nlm.2008.10.011

Van Brederode, J. F., Mulligan, K. A., & Hendrickson, A. E. (1990). Calcium-binding proteins as markers for subpopulations of GABAergic neurons in monkey striate cortex. *The Journal of Comparative Neurology*, *298*(1), 1–22. https://doi.org/10.1002/cne.902980102

van Polanen, V., & Davare, M. (2015). Interactions between dorsal and ventral streams for controlling skilled grasp. *Neuropsychologia*, *79*(Pt B), 186–191. https://doi.org/10.1016/j.neuropsychologia.2015.07.010

Verghese, P., & Beutter, B. R. (2002). Motion Processing. In V. S. Ramachandran (Ed.), *Encyclopedia of the Human Brain* (pp. 117–135). Academic Press. https://doi.org/10.1016/B0-12-227210-2/00215-6

Wang, X. J. (2006). A microcircuit model of prefrontal functions: Ying and Yang of reverberatory neurodynamics in cognition. In *The Frontal Lobes* (pp. 92–127). Cambridge University Press. https://doi.org/10.1017/CBO9780511545917.006

Wang, X.-J., Tegnér, J., Constantinidis, C., & Goldman-Rakic, P. S. (2004). Division of labor among distinct subtypes of inhibitory neurons in a cortical microcircuit of working memory. *Proceedings of the National Academy of Sciences of the United States of America*, *101*(5), 1368–1373. https://doi.org/10.1073/pnas.0305337101

Wang, X.-J., & Yang, G. R. (2018). A disinhibitory circuit motif and flexible information routing in the brain. *Current Opinion in Neurobiology*, *49*, 75–83. https://doi.org/10.1016/j.conb.2018.01.002

Yan, Y. H., van Brederode, J. F., & Hendrickson, A. E. (1995). Developmental changes in calretinin expression in GABAergic and nonGABAergic neurons in monkey striate cortex. *The Journal of Comparative Neurology*, *363*(1), 78–92. https://doi.org/10.1002/cne.903630108

Zhuang, J., Stoelzel, C. R., Bereshpolova, Y., Huff, J. M., Hei, X., Alonso, J.-M., & Swadlow, H. A. (2013). Layer 4 in primary visual cortex of the awake rabbit: Contrasting properties of simple cells and putative feedforward inhibitory interneurons. *The Journal of Neuroscience: The Official Journal of the Society for Neuroscience*, *33*(28), 11372–11389. https://doi.org/10.1523/JNEUROSCI.0863-13.2013

Curriculum Vitae

Nika Khajehdehi

EDUCATIONAL HISTORY

University College Dublin | Dublin, IR   2023 - Present
Graduate Entry Medicine

Western University | **London, ON**
Master's of Science in Physiology and Pharmacology   2019 – 2023
Bachelor of Basic Medical Sciences – Honors Specialization   2015 – 2019

TEACHING EXPERIENCE

Teaching Assistant – Western University | London, ON   Sept. 2019 – Apr. 2021
- Physiology and Pharmacology 3120

RESEARCH EXPERIENCE

Researcher | **Toronto, ON**   Apr. 2018 – Aug. 2019
- Systematic review under supervision of Dr. Ognjen Visnjevac to investigate the effects of Naltrexone on cancer progression and mortality

Researcher – Department of Biology, Western University | **London, ON**   Mar. 2017 – Nov. 2018
- Interactions between Cymbopogon citratus and Lavandula officinalis in combination with ampicillin influencing antibacterial activity on Sporosarcina ureae and Serratia liquefaciens

Researcher– Hamilton Health Sciences, McMaster University | **Hamilton, ON**   Jul. 2014 – Aug. 2016
- Assisted with characterizing psychological factors in chronic pain under supervision of Dr. Eleni Hapidou

PUBLICATIONS

Liubchenko, K., Kordbacheh, K., Khajehdehi, N., Visnjevac, T., Ma, F., Khan, J. S., Storey, M., Abd-Elsayed, A., & Visnjevac, O. (2021). Naltrexone's Impact on Cancer Progression and Mortality: A Systematic Review of Studies in Humans, Animal Models, and Cell Cultures. *Advances in therapy*, *38*(2), 904–924. https://doi.org/10.1007/s12325-020-01591-9

Araz, K.; Patel, S.; Khajehdehi, N.; Bjerkan C. W.; Thomas, J.; and Krajnyk, I. (2017). Interactions between Cymbopogon citratus and Lavandula officinalis in combination with ampicillin influencing antibacterial activity on Sporosarcina ureae and Serratia liquefaciens. *Western Undergraduate Research Journal, 9*(1). DOI: 10.5206/wurjhns.2018-19.2

AWARDS AND ACCOMPLISHMENTS

Western University | London, ON
- Dean's Honor List (2018, 2019)

RESEARCH PRESENTATIONS

Western University | London, ON

- Robarts Research Retreat – 2021
- PhysPharm Virtual Research Day – 2020